The Thesis Committee for Julie Ann Hollek

Certifies that this is the approved version of the following thesis

Hobby-Eberly Telescope Chemical Abundances of Stars in the Halo (CASH) Project - Spectroscopic Analyses of the First ~ 80 Stars

APPROVED BY
SUPERVISING COMMITTEE:

Supervisor: _____
Christopher Sneden

_____
Harriet Dinerstein

Hobby-Eberly Telescope Chemical Abundances of Stars in the Halo (CASH) Project - Spectroscopic Analyses of the First ~ 80 Stars

by

Julie Ann Hollek, B.S.

Thesis

Presented to the Faculty of the Graduate School of

The University of Texas at Austin

in Partial Fulfillment

of the Requirements

for the Degree of

Master of Arts

The University of Texas at Austin

December 2010

To Colby for weathering the crazy and Ms. Maciolek for getting me into this mess.

Acknowledgments

Julie Ann Hollek

The University of Texas at Austin

December 2010

Hobby-Eberly Telescope Chemical Abundances of Stars in the Halo (CASH) Project - Spectroscopic Analyses of the First ~ 80 Stars

Julie Ann Hollek, M.A.
The University of Texas at Austin, 2010

Supervisor: Christopher Sneden

The Hobby-Eberly Telescope Chemical Abundances of Stars in the Halo (CASH) project aims to characterize the nature of the early universe through the study of metal-poor stars in the stellar halo of the galaxy. Once completed, this will be the largest set of abundances determined for metal-poor stars from high resolution spectra. In this paper, we present chemical abundances and trends of eleven elements for the first ∼80 stars of the ∼500 star study. These 80 stars serve as a pilot sample to test the automated stellar parameter and abundance determination pipeline newly developed for the CASH project called CASHCODE. Among the pilot sample, two stars with [Fe/H]<-3.5 were discovered and their abundance analysis is discussed.

Contents

Acknowledgments **v**

Abstract **vi**

Chapter 1 Introduction **1**

Chapter 2 Stellar Sample and Observations **5**

2.1 Sample Selection 5

2.2 Observations 7

Chapter 3 Data Processing **9**

3.1 Data Reduction for CASH 9

3.2 Normalization and Radial Velocity Determination for CASH 10

3.3 Stellar Parameters and Abundances for CASH 10

3.4 AAT Data Processing 16

3.5 AAT Abundance Measurement 19

3.6 Magellan MIKE Data 20

Chapter 4 Standard Star Comparison **22**

Chapter 5 Results **26**

5.1 Abundance Trends 27

5.1.1 Light Elements: Li, C, O 27
5.1.2 Alpha Elements: Mg, Ca, Ti 31
5.1.3 Fe Peak Elements: Cr, Ni 36
5.1.4 Neutron Capture Elements: Sr, Ba 40

Chapter 6 Analysis of Two Newly Discovered EMP stars 44

6.1 HE0013-0257 45
6.1.1 Stellar Parameters 45
6.1.2 Abundances 46
6.2 HE1116-0634 50
6.2.1 Stellar Parameters 51
6.2.2 Abundances 51
6.3 Interpretation 55

Chapter 7 Conclusions 58

Vita 64

Chapter 1

Introduction

In the primordial universe, Big Bang nucleosynthesis created only hydrogen and helium with trace amounts of lithium. The first stars, Population III, formed from this metal-free material. These stars are thought to have been massive (Bromm et al., 1999), thus their chemical feedback enriched the environment from which a second generation of low-metallicity, Population II, stars formed. The atmospheres of these Population II stars contain the fossil record of the endpoints of the Population III stars, that is to say that the chemical make up of the metal-poor Population II stars was determined by supernova outbursts in the early universe. By studying the chemical abundance ratios in metal-poor stars, constraints can be placed upon the specific types of nucleosynthetic processes. By extension, we can learn about the different types of supernovae and their respective yields as well as the initial mass function of the early universe.

Metal-poor stars show great diversity in their abundance patterns, though a majority show abundance patterns similar to a scaled-down version of the solar abundances, but with an α-element enhancement and Fe peak depletion compared to solar. This signature can be explained with pre-enrichment supernova models. Efforts to classify metal-poor stars have been based on metallicity and chemical

composition (Beers & Christlieb, 2005). Stars with [Fe/H]<-3.0 are considered to be extremely metal-poor (EMP) and many have been discovered. EMP stars are likely the close descendants of the first generations of stars. As metallicity decreases the number of stars in each metallicity bin decreases; only two hyper metal-poor (HMP) [Fe/H]<-5.0 have been discovered (e.g. HE1327-2326 Frebel et al., 2005).

Beyond metallicity, chemical composition can be used to distinguish astrophysically interesting (i.e. chemically peculiar) groups of stars. One example of this is the group of so-called carbon-enhanced metal-poor (CEMP) stars. These stars show [C/Fe] >1. Detailed abundance studies have shown that $\sim$ 25% of stars with [Fe/H]<-2 are classified as CEMPs. Other chemically deviant groups which have been found are the rapid neutron capture, or r-process, enhanced stars (e.g CS22892-052 Sneden et al., 1996). The r-process is thought to have occurred in core collapse supernovae in the early universe. Slow neutron capture, or s-process, occurs in the highly evolved asymptotic giant branch (AGB) stars and the signature can be found in low-metallicity binary stars which have undergone mass transfer (e.g. CS29497-030 Sivarani et al., 2004). It also may have been put into the interstellar medium (ISM) through AGB winds. It has been discovered in many instances that the chemically peculiar stars belong to more than one of the abundance groups. Towards the lowest metallicities this becomes even more apparent: a large fraction of the stars become members of one of these chemically deviant groups. In fact, of all the known HMP stars are carbon-enhanced.

Over the past two decades, large-scale, low resolution objective prism surveys such as the HK survey Beers et al. (1985, hereby BPS) and the Hamburg/ESO survey (Christlieb, 2003) have established that these chemical outlier groups do exist. Low and medium resolution surveys can really only yield indirect information on the [Fe/H] and perhaps the α elements through the Mg b lines in medium resolution spectra (Lee et al., 2007), thus high resolution follow up is necessary to both confirm

the metallicity of the metal-poor candidates and to complete detailed abundance analysis for the stars. These studies have been successful, yielding many EMP stars which have been extensively studied at high resolution.

High resolution (R$\sim$40,000) follow up studies have been limited to $\sim$30 stars (e.g. Cayrel et al., 2004; Lai et al., 2008, hereby Lai). These studies have determined detailed chemical abundances which have been used to establish abundance trends, investigate cosmic scatter, and make comparisons to supernova nucleosynthesis yields; however obtaining high resolution, high signal-to-noise data is time-intensive because much longer exposure times are needed as R increases. A compromise between costly high resolution data and medium resolution data, which only provides macroscopic abundances, is needed because the study of individual stars is insufficient to determine a statistically robust frequency for the CEMPs and other groups of metal-poor stars. Instead, it is necessary to turn to large samples to better understand these frequencies. In particular, large studies of metal-poor stars serve multiple purposes, e.g abundance trends can be determined in a systematic, statistical manner, a more detailed understanding of galactochemical evolution can be obtained, and by extension, the occurrence rate of different nucleosynthetic processes in the early universe can be studied.

"Snapshot" spectra (R$\sim$15,000-20,000, S/N$\sim$ 60 per pixel) fill the gap between high and medium resolution. From these data, abundances over a large range of elements can be derived with moderate errors ($\sim$0.25 dex Barklem et al. (2005, hereby HERES)). One such study to do this is the HERES sample, and to date, it's the largest homogeneous set of abundances determined from high resolution spectra of metal-poor (defined as [Fe/H]<-1.5) stars, with 373 total stars and 253 published in the paper. The HERES set determined abundances (or upper limits) for 22 elements, covering a wavelength range of $\lambda \sim$ 3760-4980Åwith median S/N $\sim$54 at R$\sim$ 20,000.

The Chemical Abundances of Stars in the Halo (CASH) project is a dedicated University of Texas effort that aims to provide abundances for ∼500 metal-poor stars based on snapshot spectra taken with the High Resolution Spectrograph (Tull, 1998) on the Hobby-Eberly Telescope. We will use these abundances to address the aforementioned science questions better answered with a large, homogeneous sample.

In the process, it is expected that the majority of the stars will have ordinary halo abundance patterns, but those stars with deviating (=interesting) chemical signatures (perhaps ∼10%) will have follow up observations taken at higher resolution and S/N to study these newly discovered stars in great detail. Amongst other things, the abundances will be compared with supernova yield models (Heger & Woosley 2008) to investigate the underlying mass function of the progenitors(). Frequencies of abundance groups (e.g. CEMP, neutron-capture enhanced stars) will be determined in a statistically robust manner for the largest high resolution homogeneous sample of halo stars.

Chapter 2

Stellar Sample and Observations

2.1 Sample Selection

The stars for the CASH project were chosen from the following surveys: the Hamburg/ESO survey (HES) (Christlieb et al., 2001) (Frebel et al., 2006, hereby Frebel06), the Sloan Digital Sky Survey (SDSS) (Adelman-McCarthy, 2006), the Sloan Extension for Galactic Understanding and Exploration (SEGUE) (Adelman-McCarthy, 2008), and the HK survey (BPS) with stars observable at every season.

HES was an objective prism survey taken with the ESO-Schmidt 1m telescope at La Silla from 1990-1999 to discover quasars. The majority of the objects observed, however, were not quasars, but rather stars and made up a secondary project to evaluate the stellar content of the HES. The survey was conducted on plates at a resolution of $\sim$10Å which then were digitized and automatically scanned. Color information from the spectra was used to determine temperatures, which was used in combination with the 3933Å Ca K line (Beers et al., 1999) to pick out metal-poor candidates. Ca tracks well with [Fe/H] at low metallicities. This is due to the fact that it's an α element, which show a consistent enhancement relative to solar abundances at the low metallicities. Weak lined stars are then considered candidates.

Cool giants, however, would be overlooked if candidacy was based only on the line strength. Looking at the line strength as a function of temperature then yields many more metal-poor candidates. The bright stars of the HES (B>14) required extra processing (Frebel06) to analyze due to saturation of the photographic plates. Of the bright sample, 145 new metal-poor stars were identified and confirmed.

The discovery of a metal-poor star happens in three stages. The first of which is simply identification in a large scale, low resolution survey. The second step, once a star is identified as a weak lined candidate from inspection of the Ca K line, is to obtain a medium resolution ($\sim$1Å) spectrum. This can then be analyzed to have its Ca abundance determined spectroscopically which is related to the [Fe/H] ratio. Once the metallicity of a star is established, a high resolution spectrum must then be taken to complete the analysis to measure abundances in elements not available at medium resolution.

The HES low metallicity candidates were then observed at medium resolution to determine metallicity and high resolution follow up observations have been taken as part of many studies, including the CASH project. The HES stars in CASH are from the bright metal-poor sample. Any bright sample star that did not have high resolution spectrum taken and was observable from McDonald Observatory was included in the sample for CASH.

The HK Survey was the the first large scale objective prism survey (Beers et al., 1985) (Beers et al., 1992) initially using the Curtis Schmidt telescope at Cerro Tololo International Observatory for southern regions and later, as part of HK II, using the Burrell Schmidt telescope at Kitt Peak National Observatory for northern regions, with a resolution of $\sim$10Å. Metal-poor candidates were identified by eye from photographic plates using the strength of the Ca K line. Weak lined candidates were then followed up with medium resolution (1 Å) slit spectra follow up to measure the equivalent widths of Ca K and the Balmer lines. With no temperature

information, the HK survey candidates were preferentially dwarf stars; however, this was still successful, providing the metal-poor stars analyzed as part of the First Stars study (Cayrel et al., 2004).

The Sloan Digital Sky Survey is a photometric and spectroscopic survey using a dedicated 2.5m survey telescope at Apache Point Observatory. From SDSS-I, 150,748 stellar spectra were observed. The Sloan Extension for Galactic Understanding and Exploration (SEGUE) was part of SDSS-II and aimed specifically at characterizing the structure, formation history, and chemical evolution of the Milky Way. 240,000 spectra were taken as part of SEGUE and metallicity and stellar parameters were determined using the Sloan SEGUE Parameter Pipeline (Lee et al., 2007). SDSS and SEGUE differ from the HE and HK surveys in that they skip the first low resolution observational. The HE and HK surveys had subsequent targeted medium resolution observations, whereas SDSS and SEGUE take medium resolution spectra first. Many of the stars observed in SDSS were actually calibration objects for the main survey objectives of studying galaxies and quasars.

The stars from SDSS and SEGUE in CASH were added as the data releases came in and stellar parameters were determined from the SSPP. During the CASH observations, however, the SSPP was still under development, hence the medium resolution analysis for some of these stars does not agree with the high resolution data observed in CASH. In general, different stars from different studies were added to the observing queue throughout the duration of the CASH observations, making the sample selection an evolving process.

Also included in the sample is a set of standard metal-poor stars, which have been extensively studied in the literature at high resolution (see Table 3.1). These stars are being used as comparative tests of the CASH pipeline.

2.2 Observations

Data were obtained using the High Resolution Spectrograph on the Hobby-Eberly Telescope at McDonald Observatory at R ∼15000 from December 2006 - November 2009. The HRS is a fiber-fed spectrograph. The CASH setting uses the 316g5936 cross disperser setting with 2" fibers with 2x5 binning that leads to 3.2 pixels per resolution element.

The HRS uses two CCDs for the red and blue portions of the spectrum, and with this setting, there is a gap from 5915 - 6040 Å. The S/N per pixel ratio varies from 20-120 at 5200 Å, but the median S/N value is ∼65. The wavelength range is from 4200 - 7800 Å, or from the CH g-band to the oxygen triplet. There is substantially lower S/N for the blue end of the spectra, given the combination of the somewhat poor blue response of the HRS and the lack of blue flux for many of the objects observed in CASH, especially cool giants. The sample as a whole, range in Sloan g_{mag} ∼10.6-16.4.

Once completed, the CASH project will be the largest homogeneous set of abundances determined from high resolution spectra of metal-poor halo stars by a factor of two. In total, abundances for ∼ 500 stars that have no previously published high resolution abundances will be presented. The number of objects in the study will allow trends to be studied in a statistical manner that thus far has not been possible. In this paper, we present abundances from a pilot study of the first ∼80 stars, a majority of which are taken from the HES bright sample. This pilot sample is the second largest set of homogeneous high resolution determined abundances for metal-poor stars. Thus, the size of the pilot sample is large enough such that trends can be determined outside of the low number statistics regime.

Chapter 3

Data Processing

Given the size of the sample, it was important to automate many stages of the data reduction and analysis. The first sections of this chapter discuss the data processing of CASH. Since high resolution data exist for some stars observed in the CASH project and higher resolution comparison observations have already begun, a section at the end is dedicated to describing the data processing for those stars observed with the University College of London Echelle Spectrograph (UCLES) instrument on the Anglo-Australian Telescope (AAT).

3.1 Data Reduction for CASH

Data were reduced using the IDL pipeline REDUCE (Piskunov & Valenti 2002), which performs standard echelle reduction techniques (trimming, bias subtraction, flat fielding, order tracing, extraction). Within REDUCE, the data are wavelength calibrated using ThAr lamp exposures as points of comparison. The REDUCE pipeline was chosen over comparable IRAF by hand reduction techniques because it allowed for quick reduction of the data. A test of REDUCE versus IRAF shows that the optimized extraction in REDUCE for high S/N spectra yields an extracted

spectrum that is less noisy than that of spectrum extracted in IRAF (see Figure 8 in Piskunov & Valenti (2002)). Comparisons have been made between a by hand IRAF reduction and the REDUCE reduction of medium S/N CASH data as well. Both give comparable S/N across the spectrum and the measured equivalent widths for 121 different lines differ between the two different reductions by 3±8mÅ, which is statistically insignificant (Roederer et al., 2008).

3.2 Normalization and Radial Velocity Determination for CASH

Data were then normalized in IRAF using the continuum routine in the echelle package to take out the blaze of the echelle. Individual wavelength calibrated normalized orders were then added together using scombine to create one long 1D spectrum.

Radial velocities are also measured in IRAF using the fxcorrect and rvcorrect routines of the RV package. The barycentric correction is calculated separately to then calculate the heliocentric radial velocity. The spectra are then zero point shifted based upon the instrumental radial velocity. Stars for which observations were made on multiple nights were co-added at this stage to maximize S/N.

3.3 Stellar Parameters and Abundances for CASH

Equivalent widths are measured of atomic absorption lines in the custom written IDL routine ew (Roederer et al. , in prep). The program automatically determines the continuum level and then fits a Voigt profile to each feature, as shown in Figure 3.1. The user can then change the fit by adjusting the continuum level, the width of the fit, or the line center. Automating equivalent width measurement routines is difficult, hence this is done in semi-automated way.

For lines which cannot be distinguished from noise, the S/N ratio can be

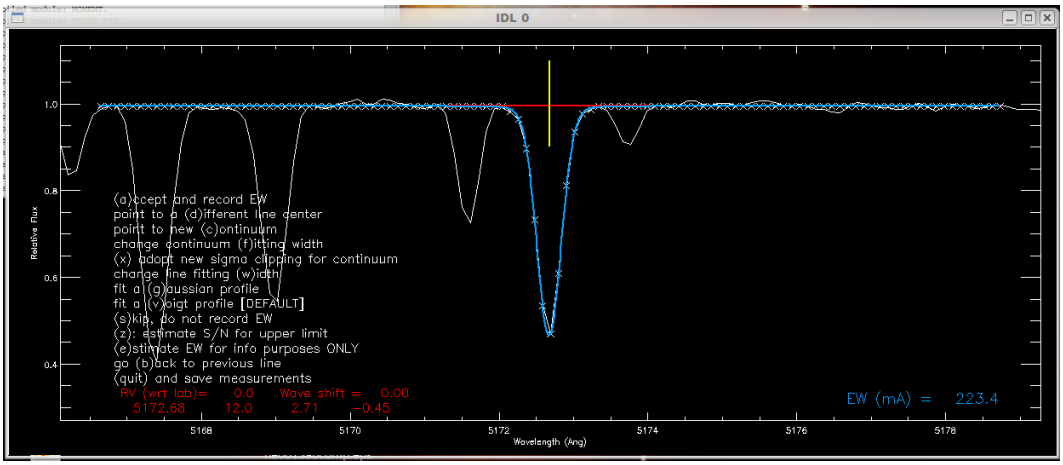

Figure 3.1 Screen shot of the IDL ew equivalent width routine. This is the 5172 Å Mg line in the star BD +17 3248.

measured in the line region, which is then used to determine an upper limit. It is then given a "u" flag to denote upper limit. For each line measured, the user chooses an "l" or "s" for lines from which the equivalent width will be used to determine abundances or for the equivalent widths which will be used in combination with spectral synthesis to determine abundances, respectively. These flags are then used by the automated stellar parameter and abundance pipeline, batch-mode MOOG.

The newly created batch-mode MOOG (hereby CASHCODE) was written around the latest update of the spectral analysis code MOOG (2009) (Sneden, 1973) to deal with large sets of data. CASHCODE is used in place of by hand analysis techniques, though extensive testing has been performed to ensure that it gives the same results. This allows for faster analysis of the data, where by hand measurements would not yield errors much smaller than the CASHCODE pipeline given the nature of the data (i.e. low S/N at R∼15000). The CASHCODE pipeline, however, requires no interaction beyond the compilation of an input file.

CASHCODE iteratively determines the stellar parameters and then determines abundances from equivalent widths (l flags), synthesis (s flags), and 3σ upper

limits (u flags). In this case, the upper limit is calculated using the same prescription as Norris et al. (2002), where $\sigma = \lambda(n_{pix})^{1/2}/R(S/N)$, where R is the resolution, S/N is per pixel, λ is the wavelength and n_{pix} is the number of pixels over the line.

Stellar parameters are determined using the Fe I, Fe II and Ti I, Ti II lines, though the user can specify the use of only Fe or only Ti in the input file. In the standard case when both Fe and Ti are used, Fe is weighted twice that of Ti in considering the derivation of the stellar parameters. Spectroscopic effective temperatures are determined by demanding no trend in the derived abundances versus the excitation potential. Surface gravity, log g, is determined by demanding that both the ionized and neutral species of an element give the same abundance. Microturbulence is derived by demanding that there is no trend between reduced equivalent width, which is the equivalent width of a line divided by its wavelength, and abundance; that is to say that both strong and weak lines of the same species should derive the same abundances. Metallicity is determined from the derived abundances relative to solar. This takes into consideration both Fe and Ti unless otherwise indicated.

The user inputs an initial guess to each parameter and then the code evaluates the slopes of the Δ log(ϵ) versus excitation potential for T_{eff}, Δ log(ϵ) versus log(RW) for microturbulence, the derived abundances for particular ionization states, and the overall metallicity derived for a given iteration. The user also indicates the criteria for how much error is allowed in determining the different stellar parameters. See Table 3.1 for the specific set of parameters used for CASH. CASHCODE generates plots of these quantities for visual inspection during the stellar parameter determination portion of the pipeline, as seen in Figure 3.2. In this case, Δ log(ϵ) is the derived log(ϵ) abundance for a specific ionization state and element - average abundance determined for the given species. This is done so that elements that greatly differ in their absolute log(ϵ) abundances can be compared on the same

scale. If the slopes are not within a specified range or there is a large discrepancy between two species (e.g. Fe I and Fe II) or there is a large discrepancy between the model atmosphere abundance and the derived abundance, another iteration is performed adjusting T_{eff}, log g and microturbulence. For cases where a particular parameter is grossly deviant, then only that parameter is changed and the entire set of parameters is again evaluated. Metallicity is evaluated at each iteration. If the derived metallicity is off by a specified amount compared to the model, a new metallicity is determined for the next iteration. Once the code has iterated to satisfactory parameters, the model atmosphere is then used for the abundance determination. Model atmospheres, in this case 1D LTE Castelli-Kurucz models, with α enhancement (Castelli & Kurucz, 2004).

The stellar parameters determined for the first set of stars are plotted in an HR diagram form in Figure 3.3. Over plotted are Yale-Yonsei (Kim et al., 2002) isochrones. The horizontal branch is a mass sequence from Cassisi et al. (2004). The black solid line is an isochrone for 12 Gyr at a metallicity of [Fe/H]=-2.5. Plotted in blue is a 12 Gyr isochrone at [Fe/H]=-3.0 and the red line is another 12 Gyr isochrone for [Fe/H]=-2.0. Plotted along with the CASH stars are those from the HERES sample (green exes) and the Lai sample (cyan exes). The CASH sample scatters around the isochrone fairly well with a few exceptions, though they fall near the isochrone within the errors. Thus, a qualitative check of the CASHCODE pipeline shows that the determined stellar parameters make sense. More rigorous testing was performed and will be discussed in Chapter 4.

Lines with the l flag denote abundances determined using the abfind driver in MOOG. These abundances are based on a curve of growth analysis using the equivalent widths measured for a species.

Lines with the s flag denote abundances determined using the synth driver in MOOG. For these lines, it takes the equivalent width determined abundance and

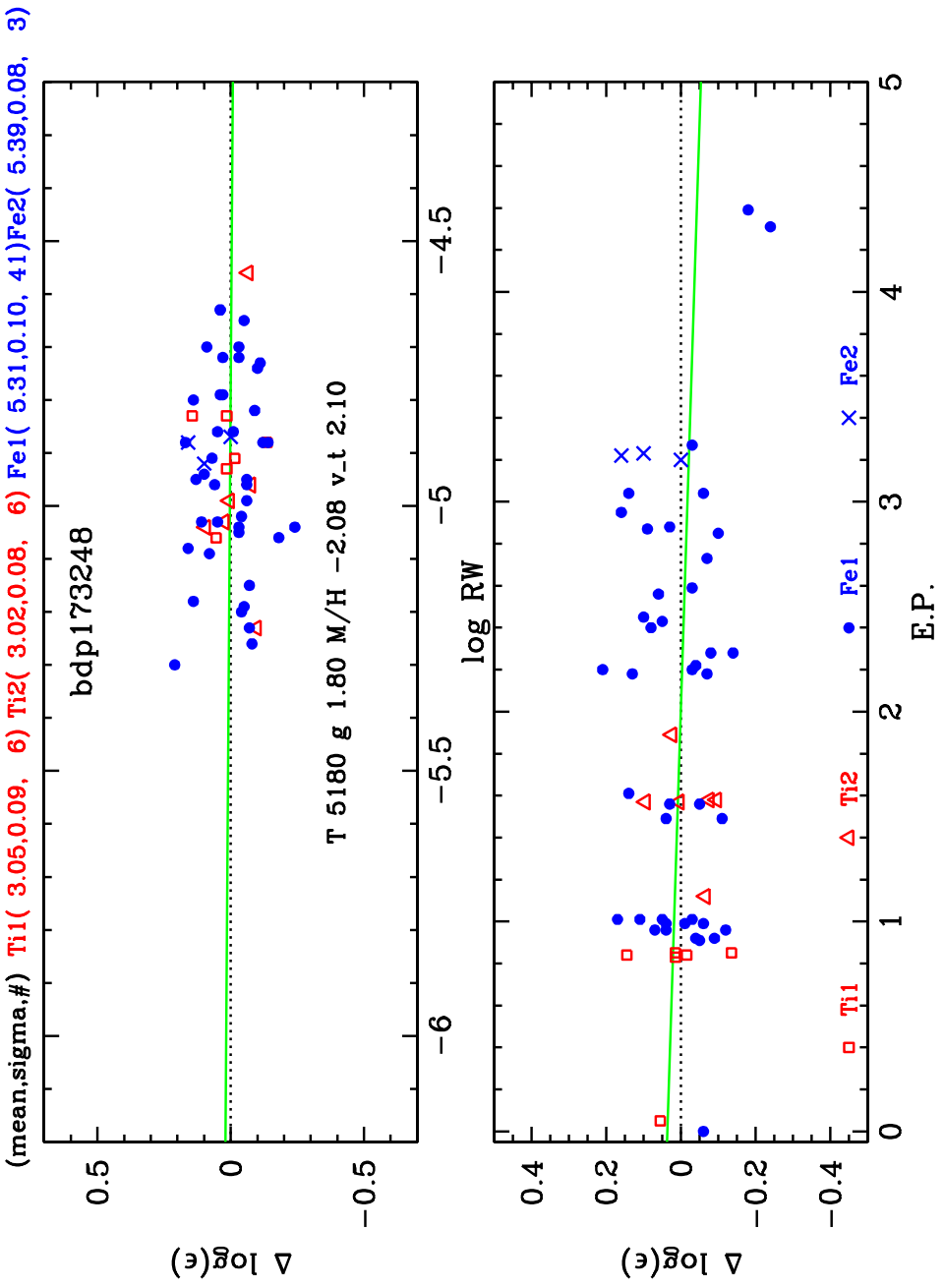

Figure 3.2 This is an example of a CASHCODE pipeline plot which is shown during the evaluation of the stellar parameters. In the upper plot, $\Delta\log(\epsilon)$ is plotted against log RW. From this, the microturbulence is determined. In the bottom plot, the excitation potential is plotted against $\Delta\log(\epsilon)$. From this, the spectroscopic effective temperature is calculated.

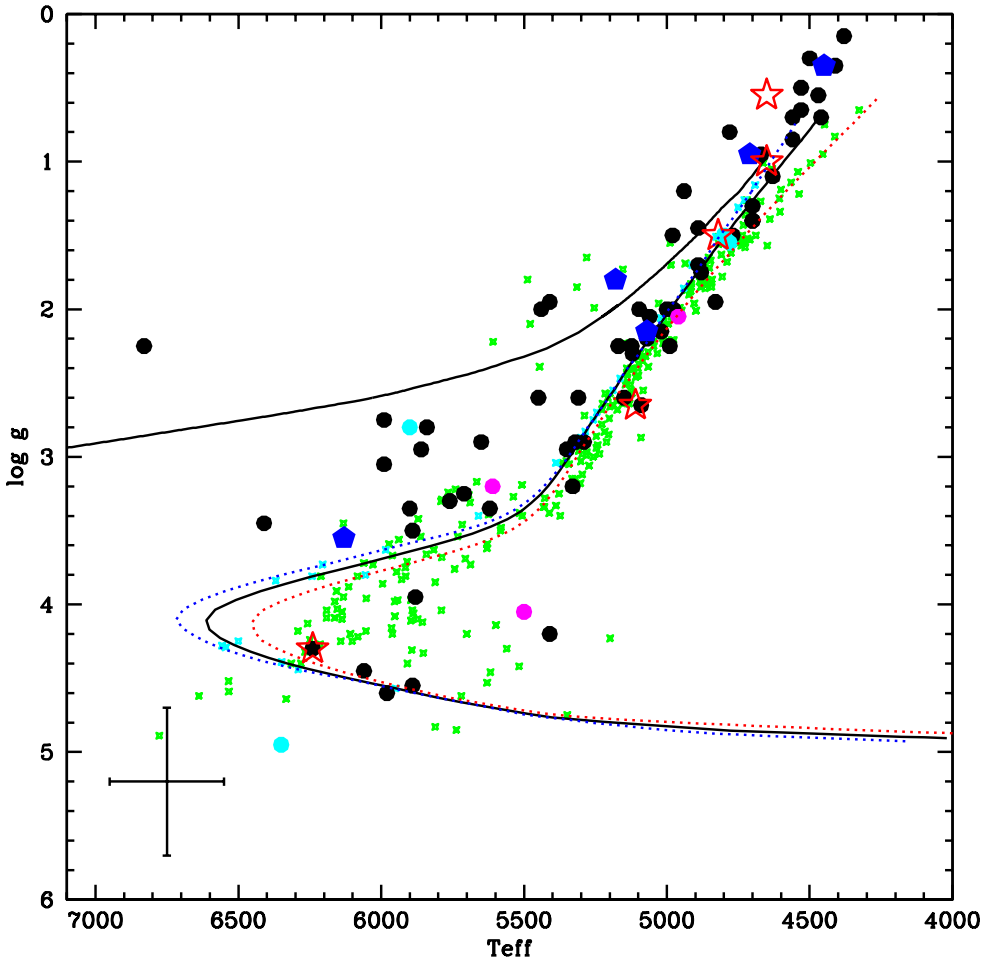

Figure 3.3 HR diagram of CASH stars, plotted with 12 Gyr Yale-Yonsei isochrones plotted in red for [Fe/H]=-2.0, black for [Fe/H]=-2.5, and blue for [Fe/H]=-3.0 and a Cassisi horizontal branch. Different samples correspond to different colors. The black circles are from HES, the pink circles are from HK, the cyan circles are from SDSS, and the red open stars are HES stars for which AAT data have been taken. The blue pentagons refer to standard stars within the CASH sample. The cyan exes are the stellar parameters of stars in the Lai study and the green exes are stars from the HERES study.

creates a synthetic spectrum. It also synthesizes other synthetic spectra centered around the equivalent width guess. χ^2 minimization is used to determine the best fit abundance. An example of a CASHCODE synthesis for the 4215 Å Sr line is shown in Figure 3.4.

The line list was adopted from Roederer et al. (2010), using updated oscillator strengths in (e.g. Cr I (Sobeck et al., 2007) and Fe II (Meléndez & Barbuy, 2009)) and omitting lines that cannot be properly measured at R$\sim$15000. In total, 113 lines make up the line list, though not all lines are measured in each star.

For a typical star, 16 abundances can be determined: Mg, Ca, Sc, Ti, Cr, Mn, Fe, Ni (from equivalent widths) and Li, C, O, Zn, Zr, Sr, Y, Ba (from synthesis). We report only Li, C, O, Mg, Ca, Ti, Cr, Fe, Ni, Sr, and Ba as those are element which seem to give robust abundances. Work is being made to the line list to achieve the same precision from Sc, Mn, Zn, Zr, and Y; however there are limitations to these data based on the S/N, resolution, and wavelength coverage. Sc has four lines in the CASH wavelength regime. Abundances derived from these lines vary widely. A differential line analysis will be performed to reevaluate the errors on the Sc abundances. Once this is performed, the Sc abundances will be considered with the rest.

The one element which is not part of the CASHCODE is C. The CH g-bandhead feature at 4313 Å is used to determine the C abundance. This is in a region of the spectrum which is low S/N in the CASH data, making continuum placement difficult, so this synthesis is done by hand using the stand alone version of MOOG. Figure 3.5 shows an example of a by hand C synthesis for CASH data.

3.4 AAT Data Processing

Five stars from the bright sample of the HES were observed with the UCLES instrument on the AAT in April 2005; those data were not analyzed. Since high

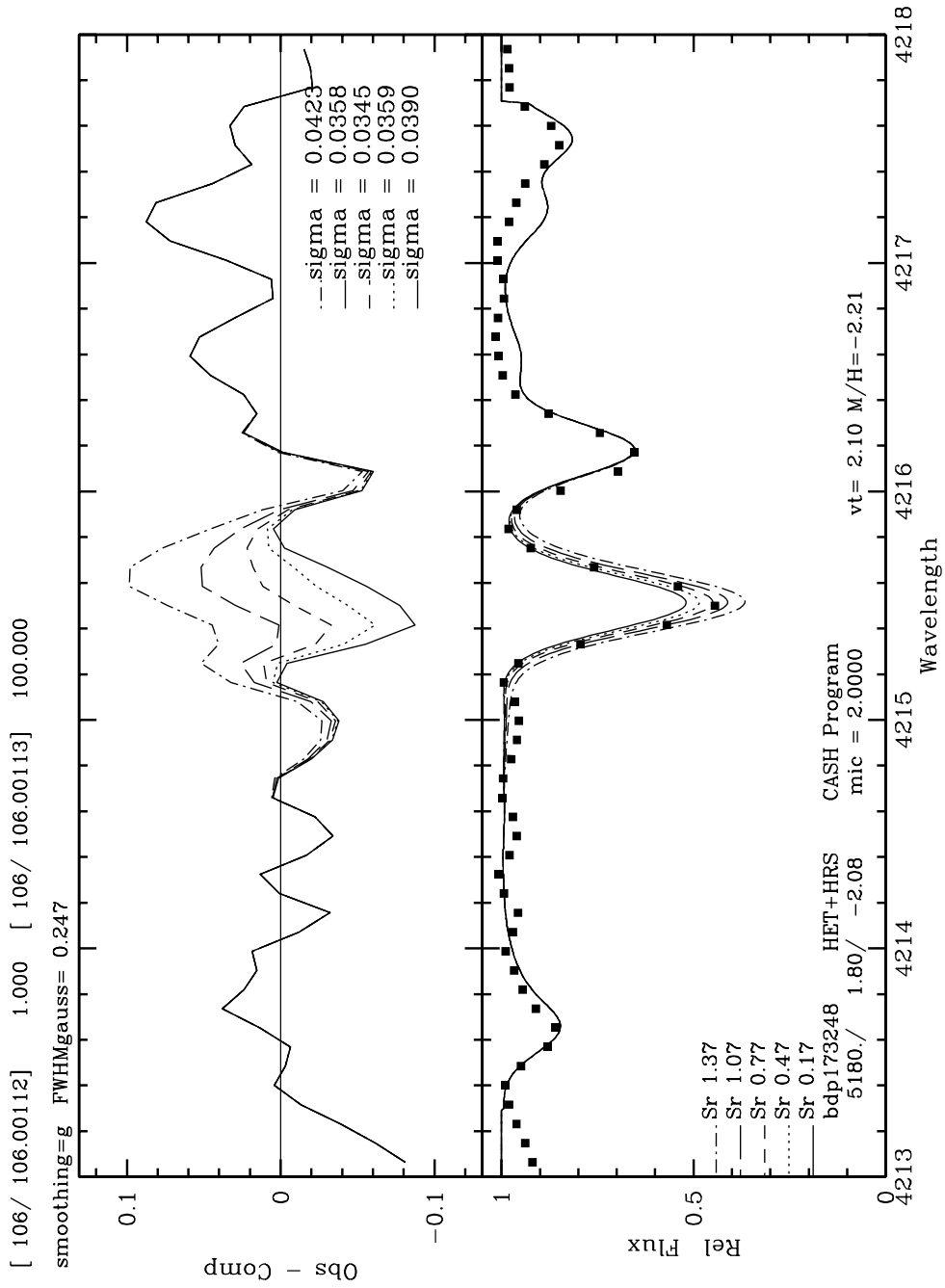

Figure 3.4 Plot of a spectral synthesis for the 4215Å Sr feature for BD+17 3248. This plot is automatically created during the synthesis portion of CASHCODE.

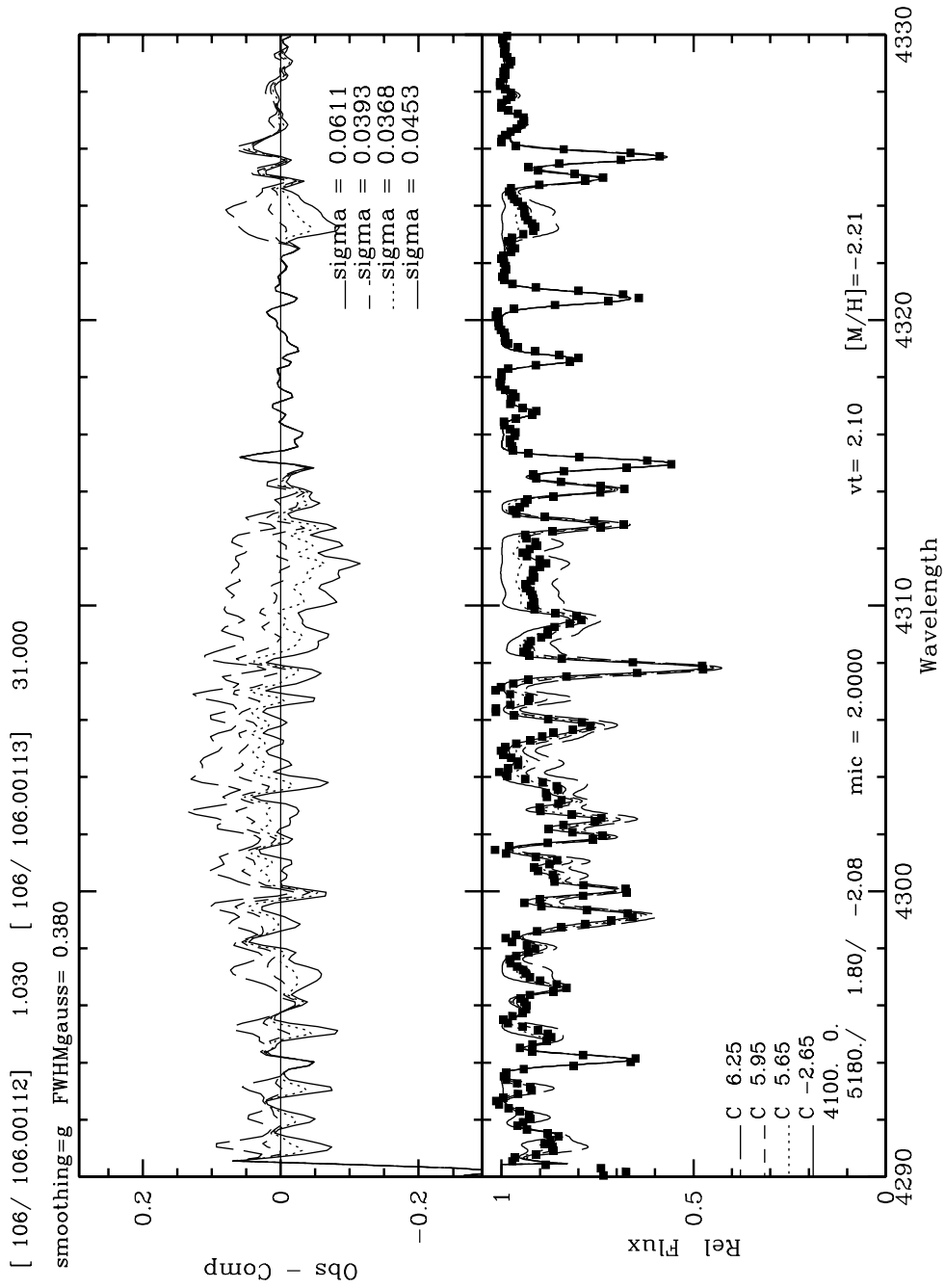

Figure 3.5 By-hand synthesis of the CH g-bandhead region for BD +17 3248. The C abundances are determined using the features at ∼4310Å and ∼4323 Å.

resolution data of these objects were observed before the CASH observations, these stars were fed into the CASH program as points of comparison between the high resolution data and the snapshot data. These data are more than just comparison stars, however; they are all metal-poor with interesting abundance signatures and merit investigation beyond use as a comparison tool. The wavelength coverage spans from 3710-4950Å at R$\sim$20,000. Given the much bluer wavelength coverage of the AAT data, comparison with CASH serves as a way to determine how the use of different lines of the same elements will affect the derived stellar parameters and abundances.

Data were reduced by hand, as opposed to in a pipeline, with IRAF, using the echelle package. Standard echelle reduction techniques were applied, including trimming, bias subtraction, and flat fielding. Once the objects were flat fielded, l.a. cosmic (van Dokkum, 2001) was used to remove cosmic ray hits. The data were then extracted and wavelength calibrated, using ThAr lamps. The individual wavelength calibrated orders were then combined to make a 1D spectrum in the same method as the CASH data.

3.5 AAT Abundance Measurement

Equivalent widths were measured using a specialized Midas program called gauss-fit, which automatically determines the continuum and fits Gaussian profiles to lines. The user can then modify the fit by specifying which regions over which to calculate the continuum and the width and center of the line. This differs from ew in that the fit from ew is a Voigt profile, which will make a difference in strong lines, and the continuum isn't calculated by the user, but rather the level can be adjusted by hand. It is essential in ew for the continuum to be well normalized. gauss-fit allows for multi-order fits to be made to calculate a continuum. We chose to use a linear fit, allowing the program to calculate a continuum with a slope, but no other higher

order features. Comparison between the two programs has shown that ew measures larger equivalent widths for strong lines, but this is expected since the wings are fit with a Lorentzian profile in ew and are not in gauss-fit. The line list for these stars was compiled based on Aoki et al. (2007) and the lines from Roederer et al. (2010). The oscillator strength from Roederer et al. (2010) was chosen in cases where there were two of the same feature with different measurements in the list.

Stellar parameters were then measured by hand, using the Fe I and Fe II lines using the abfind driver in the latest version of MOOG. This driver is also used to determine the abundances based upon the measured equivalent widths. The synth driver in MOOG is then employed to perform spectral synthesis for Ba II, Sr II, and the CH g-band features.

3.6 Magellan MIKE Data

Observations of a set of stars observed in CASH were taken using the Magellan MIKE (Bernstein et al., 2003) instrument prior to the CASH program, but the addition of more observations is underway to enlarge the comparison sample. Again, these stars were included in CASH as a way to test the pipeline with new data. In addition high resolution (R$\sim$35000) and high S/N observations of interesting CASH stars using the MIKE instrument have already been taken. The wavelength coverage of MIKE is from 3500-9000Å. This covers both the AAT and CASH wavelength regimes. These data were reduced using the an IDL pipeline made for MIKE (D. Kelson, private communication, reduced by A. Frebel), equivalent width measured using the gauss-fit program and the same AAT line list, and abundance analyzed using MOOG.

Analysis of the MIKE stars and the AAT stars is still underway. Once the entire CASH study is completed, these stars will provide points of comparison for the CASH sample in addition to being scientifically interesting based upon their

abundances.

Chapter 4

Standard Star Comparison

Six bright, well studied stars were observed as part of the CASH program. These stars were reduced and analyzed in the CASH pipeline. In order to compare the pipeline results to the literature values, the equivalent widths were first compared to other studies. Since equivalent widths are measured by hand, careful consideration must be made with respect to the continuum placement, as it is a user-defined quantity and can lead to errors. Comparison to other studies (e.g. Fulbright (2000) in Figure 4.1) have shown that the measurements made in CASH are essentially the same as other studies, with the average mean difference between CASH and Fulbright being 2.4±3.4 mÅ, which is negligible and therefore should derive the same stellar parameters with the same techniques.

To test the stellar parameter pipeline, we compared the stellar parameters from other high resolution spectroscopic studies. Figure 4.2 shows the residual plots of the stellar parameters from comparison, as well as an HR diagram of the standard star sample. These six stars were chosen because they span a range in the HR diagram. For BD +17 3248 and HD 140283, we find good agreement between high resolution and CASH stellar parameters. We find less agreement for other stars with the mean Δ T_{eff} = -24 ±10 K, the mean Δ log g = -0.02 ±0.04 , and the mean

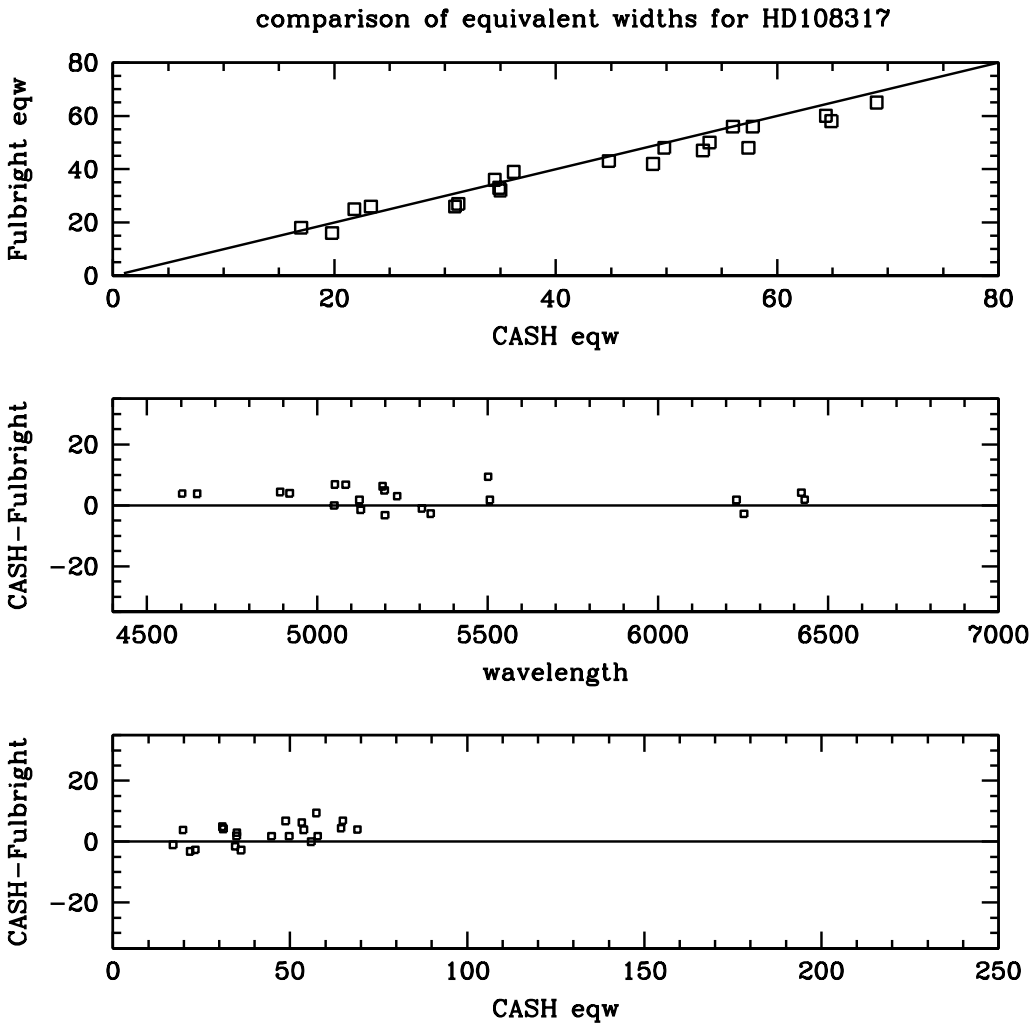

Figure 4.1 Comparison of the equivalent widths measured from CASH data and from similar resolution data from Fulbright (2000). In the first panel the equivalent widths from CASH and Fulbright are plotted against each other. In the second panel, the residuals are plotted against wavelength and in the third panel, residuals are plotted against the equivalent width measured in CASH. The slope in this panel shows that CASH measures larger equivalent widths with larger lines. This is likely due to the differences in measurement tools, as ew measures a Voigt profile and IRAF measures Gaussians.

Table 4.1. List of Standard Stars in CASH

Name	T_{eff}	log g	[Fe/H]
BD +07 3248	5180	1.80	-2.21
HD 84397	6130	3.55	-2.36
HD 108317	5110	2.34	-2.56
HD 115444	4710	0.95	-3.09
HD 122563	4450	0.35	-2.86
HD 140283	5630	3.30	-2.71

Δ [Fe/H] = -0.18$\pm$ 0.02 calculated for the six standard stars. These all fall within the errors of the CASH parameters: 150 K, 0.2 dex, and 0.2 dex for $T_{\rm eff}$, log g, and [Fe/H] respectively.

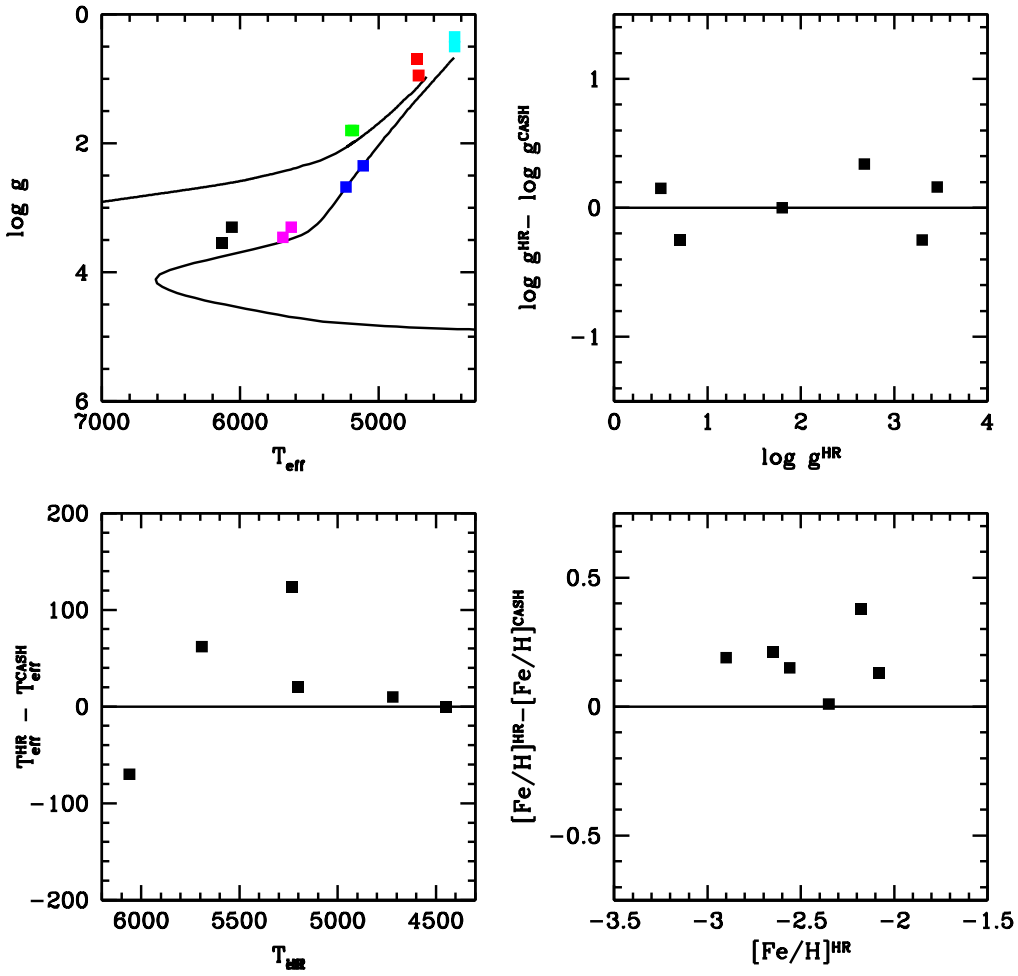

Figure 4.2 Comparison of the stellar parameters measured from CASH data and from higher resolution data from the sources cited in Table 2.1. The different colors on the symbols represent different stars: green is BD +17 3248, cyan is HD 122563, magenta is HD 140283, red is HD 115444, and black is HD 84937.

Chapter 5

Results

This chapter is comprised of a discussion of the first general abundance trends for the CASH sample for 10 different elements. For each plot, a four panel plot is shown. Panel A contains a histogram of the logϵ(X) abundances and describes the distribution of the derived abundances for a particular element X. Panel B shows [X/Fe] plotted against effective temperature. This allows for a visual determination of temperature dependencies of any given element. In particular, it was useful for reconfirming the NLTE effects in the O triplet. Panel C shows the logϵ(X) abundance plotted against [Fe/H], which describes how element X trends with metallicity. Panel D shows [X/Fe] plotted against [Fe/H]. This is the standard representation of elemental abundances. It is useful because it shows the trends of the ratio of of an element to the metallicity as a function of metallicity. As metallicity decreases, the absolute abundance of an element is also expected to decrease, with some amount of cosmic scatter. Thus normalizing to Fe allows for second order trends to be examined.

Trend lines are calculated for each abundance using a linear least squares fit with the corresponding σ calculated as well. For each elemental abundance, an "average" abundance,$[X/Fe]_{av}$ is calculated. This is the mean of [X/Fe] over all

stars in a given sample with a standard deviation, σ_{sd},also calculated. For elements that show no dependence on metallicity, this number is a useful characterization of a particular sample, though for elements with a metallicity dependence (e.g. Cr), the slope of the trend line is a much better characterization of the sample.

When available, comparison trends (i.e. slopes) or $[X/Fe]_{av}$ and the associated σ to the HERES survey and the Lai sample are given. The HERES survey is similar to CASH in resolution, but differs in wavelength coverage. This is the most comparable survey to CASH. The Lai sample is higher resolution for a smaller set of data and also differs in wavelength coverage.

5.1 Abundance Trends

5.1.1 Light Elements: Li, C, O

The Spite plateau (Spite & Spite, 1982) is an observational discovery made regarding Li abundances as a function of temperature. It was shown that in low metallicity stars of $T_{eff} > 5500$ K, the lithium abundance appeared constant. The Li abundance in metal-poor stars of these temperatures is not depleted from post main sequence convection; it is therefore thought that the stars that populate the Spite plateau contain the Li abundance of the ISM from which they formed. This lithium abundance is representative of the Li produced in Big Bang nucleosynthesis (BBN). WMAP values in combination with BBN yields for Li give A(Li)=2.6 dex, while the Spite plateau lies around 2.2 dex. This indicates that something during stellar evolution has depleted the Li abundance.

Figure 5.1 show the Li abundances. This plot is slightly different than described above. In panels B and D, the Li abundance is offset with respect to the Spite plateau rather than Fe. The abundances of the 6707Å Li doublet are measured in CASH data via spectral synthesis. The Spite plateau is clearly seen in the data

for stars of $T_{eff} > 5500$ K. For these stars, there is an internal scatter of 0.11 dex. Cooler stars show depletion of Li, which is expected given the low temperatures at which Li burns ($2.5x10^6$ K) and the onset of convection beyond the main sequence. These stars have a scatter of σ=0.26 around a slope of 0.31. There has been debate that the Spite plateau has a slope (Ryan et al., 1996, e.g.). Given the constraints on resolution and S/N, it will be difficult for CASH to enter the debate, though a slope of 0.04 $\pm$0.11 is calculated from a linear least squares fit to the Spite plateau is seen.

Carbon abundances were determined via by hand synthesis of the CH g-band around 4300 Å. Figure 5.2 shows great spread in the abundance ratio of [C/Fe] as a function of [Fe/H], with $\sigma_{sd} = 0.38$ in CASH and 0.51 in HERES. The large scatter is not only due to the quality of the analysis, but also to the cosmic scatter of C, as there are several sites of C formation in the early universe. Carbon abundances are of interest in cosmology as the number of CEMP stars found indicate that C probably played some role in early nucleosynthesis. CEMP stars fall into four categories: CEMP-s, CEMP-r, CEMP-rs, CEMP-no, with the subscripts indicating an enhancement in other groups of elements with r corresponding with the r-process, s with the s-process and "no" meaning that the star is simply C-enhanced. It is thought that the C enhancement in CEMP-s stars can be explained by mass transfer from an AGB companion. CEMP-rs stars can also be explained by mass transfer and long term radial velocity studies of CEMP-s and CEMP-rs stars have shown that there are velocity variations indicating a companion (Masseron et al., 2010, and the references within).

Oxygen is seen to be overabundant in metal-poor stars as well, on the same scale as the α-elements. Oxygen abundances are difficult to pin down given the available indicators: the OH features near the atmospheric cutoff, the forbidden line at 6300Å, and the O triplet. Each of these indicators yields different abundances.

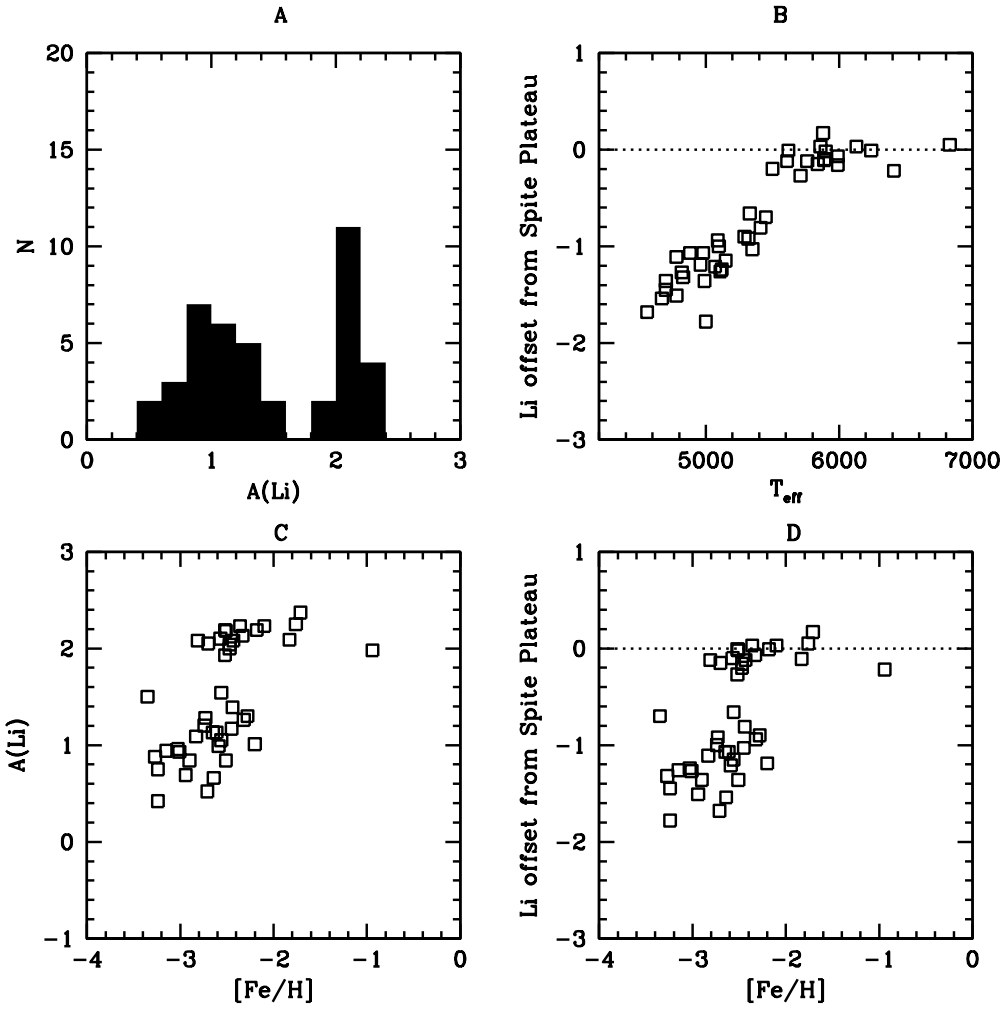

Figure 5.1 Plot of the Li abundances. The upper left panel contains a histogram of the Li abundances. In the upper right panel, Li abundances offset with respect to the Spite plateau are plotted as a function of effective temperature, with the dotted line representing the Spite plateau. In the lower left panel, A(Li) is plotted against [Fe/H] showing a large scatter in abundances. The lower right panel shows the Li abundances offset with respect to the Spite plateau plotted against [Fe/H], with the dashed line again representing the Spite plateau.

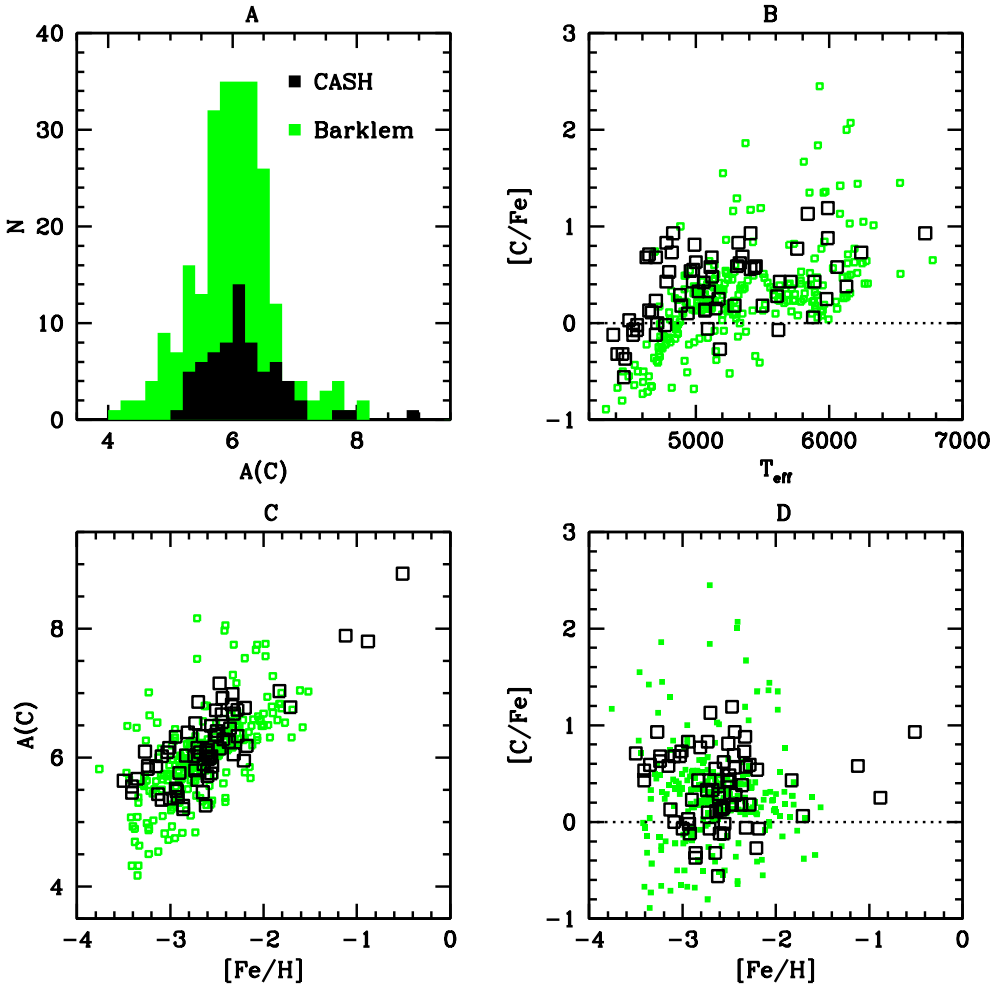

Figure 5.2 Plot of the C abundances. The upper left panel contains a histogram of the log ϵ C abundances. In the upper right panel, the [C/Fe] ratio is plotted against effective temperature, with the dotted line representing the solar ratio. In the lower left panel, logϵ C is plotted against [Fe/H] showing a correlation between C and Fe. The lower right panel shows [C/Fe]plotted against [Fe/H], with the dashed line again representing the solar ratio. This panel is is the standard way abundances are presented. Subsequent plots have the same panels. Points plotted in black are from the CASH sample and points in green are from HERES.

In the CASH sample, synthesis of the O triplet was used to determine abundances; however, it has been shown that these high excitation potential features have NLTE effects which must be accounted for to determine the the actual abundance. It is easy to see this in Figure 5.3. The disagreement between the CASH and Lai samples stems from the use of different indicators. The Lai study used OH features near the atmospheric cut-off, which have been shown to give lower abundances than the O triplet for a given metallicity and temperature (García Pérez et al., 2006).

The [O/Fe] ratio versus [Fe/H] gives slopes of -0.45±0.19 and -0.19±0.17 for CASH and Lai respectively. The mean abundance for [O/Fe] are close for the two studies at 0.80±0.33 and 0.83±0.20, but this number has a large standard deviation and must be interpreted with care. In CASH, this scatter is due to the NLTE effects which have temperature dependencies. The listed values for O derived for CASH stars have not yet been NLTE corrected.

5.1.2 Alpha Elements: Mg, Ca, Ti

It has been established that the α elements are overabundant compared to Fe (e.g. McWilliam 1997). This has been explained by the occurrence of core collapse supernovae in the early universe, which produce an underabundance of Fe compared to the α elements. Later generations of supernovae, specifically Type Ia, yield lower α abundances, driving down the [α/Fe] ratio to what we see today in the sun and similar young, metal-rich stars. The α elements are created both in core collapse supernova and also through stellar nucleosynthesis in high mass stars.

The Mg abundances are plotted in Figure 5.5. In CASH, α-enhancement is seen at the 0.43±0.21 level in Mg. $[Mg/Fe]_{av}$ in both the HERES and Lai are 0.28±0.13 and 0.28±0.15 dex respectively. This discrepancy would be well within the errors of the CASH sample for an individual star, but as a whole there is a systematic offset between CASH and the two samples. The standard deviation of

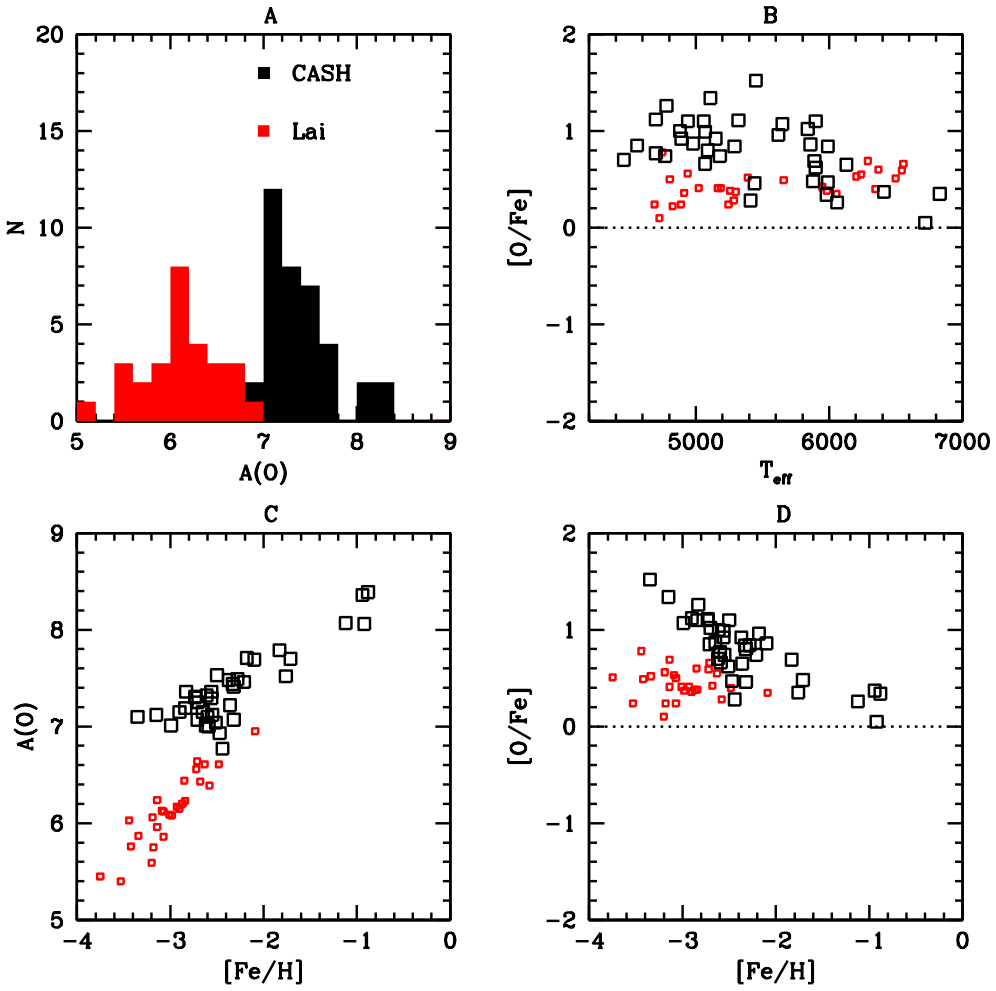

Figure 5.3 Plot of the O abundances. In the upper right panel, [O/Fe] seemingly shows a temperature dependence. There also is a discrepancy between Lai and CASH likely due to data quality, chosen indicator, and NLTE effects.

the mean for CASH is 0.02 and 0.01 for CASH and HERES. A possible cause for this discrepancy may arise from the abundance determination methods. Lai used equivalent width measurements using SPECTRE, which fits Gaussian profiles. The Mg lines available in CASH tend to be strong lines, for which ew will fit a Voigt profile, which is larger than the Gaussian that would be fit for that same line.

The HERES abundances were determined using Spectroscopy Made Easy (SME) program which determined abundances using synthetic spectra. HERES found difference between the [Mg/Fe] derived from SME and from standard equivalent width techniques (Norris et al., 1996). For strong lines, SME ignores the core and fits only the wings.

While it was expected that Mg would be overabundant, we found one star, HE 0434+0105, that seemed to be depleted in Mg. A few other metal-poor Mg-poor stars have been discovered (Ivans et al., 2003), but it's a relatively rare phenomenon, so this star had follow up observations taken with Magellan using the MIKE instrument. It was discovered that this star was a double lined spectroscopic binary thus it appeared to have a low Mg abundance. In future work both components will be abundance measured, though it is likely that both components have the normal α enhancement.

Figure 5.6 shows that calcium is also enhanced relative to solar. HERES finds $[\mathrm{Ca/Fe}]_{\mathrm{av}} = 0.27 \pm 0.11$, Lai finds $[\mathrm{Ca/Fe}] = 0.34 \pm 0.10$ and CASH finds $[\mathrm{Ca/Fe}] = 0.37 \pm 0.14$. Again there is a discrepancy between CASH and HERES at the 0.1 dex level. Given that the CASH determined Ca abundances were derived from equivalent widths and the HERES abundances were determined using SME with different lines, there is a difference in technique that can contribute to this difference.

Titanium acts as a transition between the α-elements and the Fe-peak elements. It tends to track with the α-elements, being overabundant in CASH with $[\mathrm{Ti/Fe}]_{\mathrm{av}} = 0.22 \pm 0.19$ and 0.25 ± 0.13 in HERES. There is good agreement between

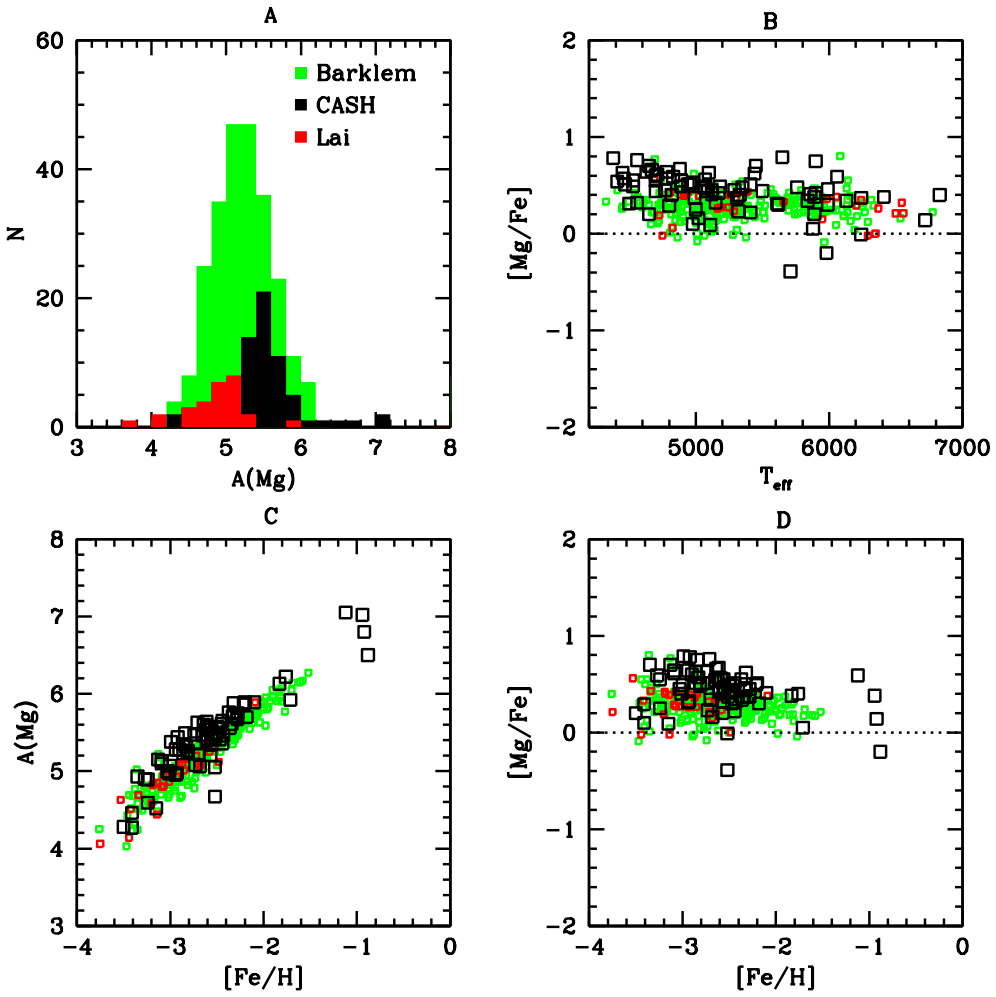

Figure 5.4 Plot of the Mg abundances. Mg is found to be overabundant compared to solar. One notable exception appears to be HE0434+0105, but that star was discovered to be a double lined spectroscopic binary.

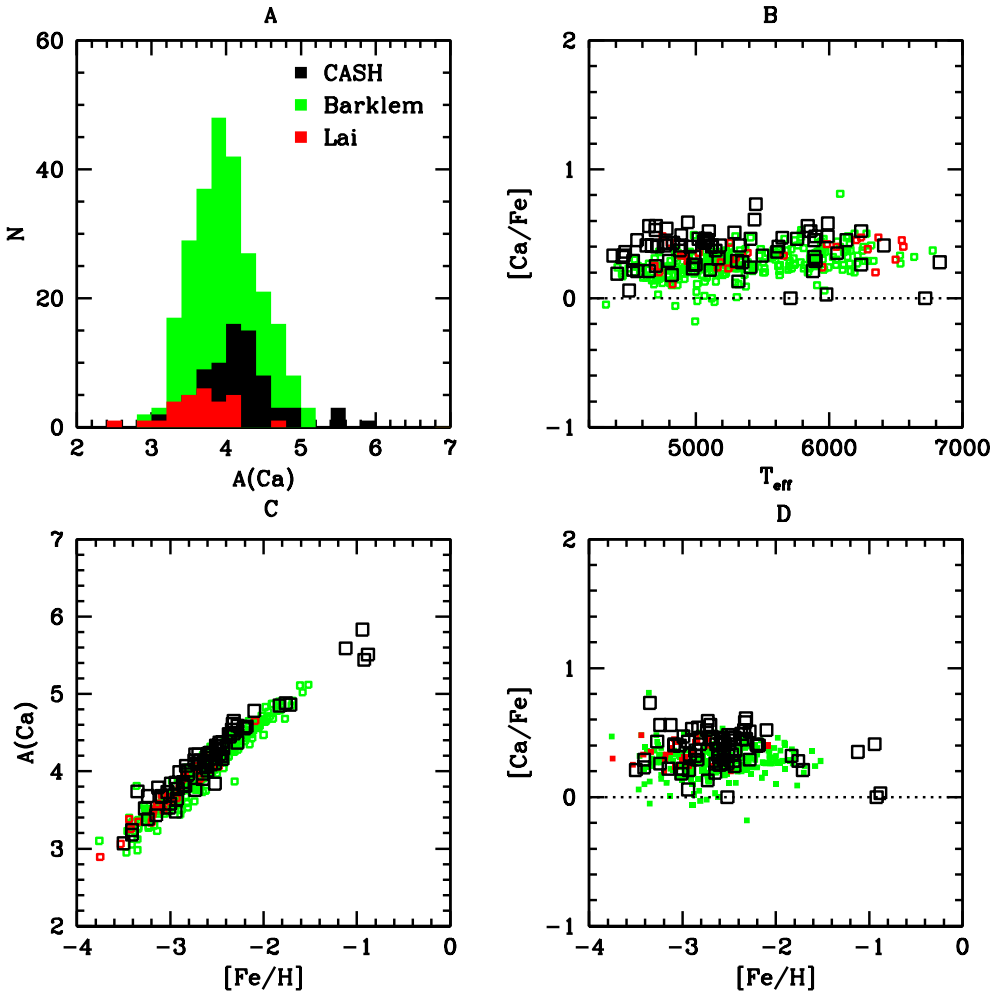

Figure 5.5 Plot of the Ca abundances, which are also overabundant compared to solar.

the abundances determined by equivalent widths (CASH) and synthesis (HERES). In Figure 5.7 it can be seen that the Lai sample shows $[Ti/Fe]_{av}$ = 0.44±0.15, which is substantially higher than CASH and HERES. This may be due to the use of different lines to determine the Ti abundance between Lai and CASH and Lai and HERES. This also may have to do with sample selection. The metallicity distributions for CASH, HERES, and Lai are all more metal-poor than the average metallicity of the halo (at [Fe/H]=-1.6). These stars were chosen to investigate the metal-poor tail of the halo. The Lai sample is peaked at the lowest metallicities at [Fe/H]∼-3.1. Towards the lowest metallicities, stars become increasingly chemically deviant.

5.1.3 Fe Peak Elements: Cr, Ni

The Fe peak elements included in CASH are Cr and Ni. The Fe peak group is interesting because they are created in supernovae, so studying their abundances provides an additional indirect probe of supernova physics.

Chromium has been found to be underabundant compared to Solar (e.g. McWilliam (1997)). HERES finds this same trend, and the [Cr/Fe] ratio seems to drop towards the lowest metallicities. This trend is less pronounced in the CASH data as seen in Figure 5.8. The slope for Cr in the CASH sample is 0.07±0.17 whereas it is much larger in HERES and Lai at 0.39±0.13 and 0.63 ±0.11 respectively. Once the CASH sample is complete, this trend can be more robustly evaluated. Since publication of the HERES paper, new values for the oscillator strengths of Cr have been published (Sobeck et al. (2007), Nilsson et al. (2006)).

Nickel abundances between CASH and Barklem are offset with $[Ni/Fe]_{av}$ = 0.22 ±0.21 for CASH, -0.02±0.19 for Barklem, and 0.05±0.10, as can easily be seen in Figure 5.9. This may be due to the differences in oscillator strengths used, although it should be noted that in CASH there are only two Ni lines available:λ

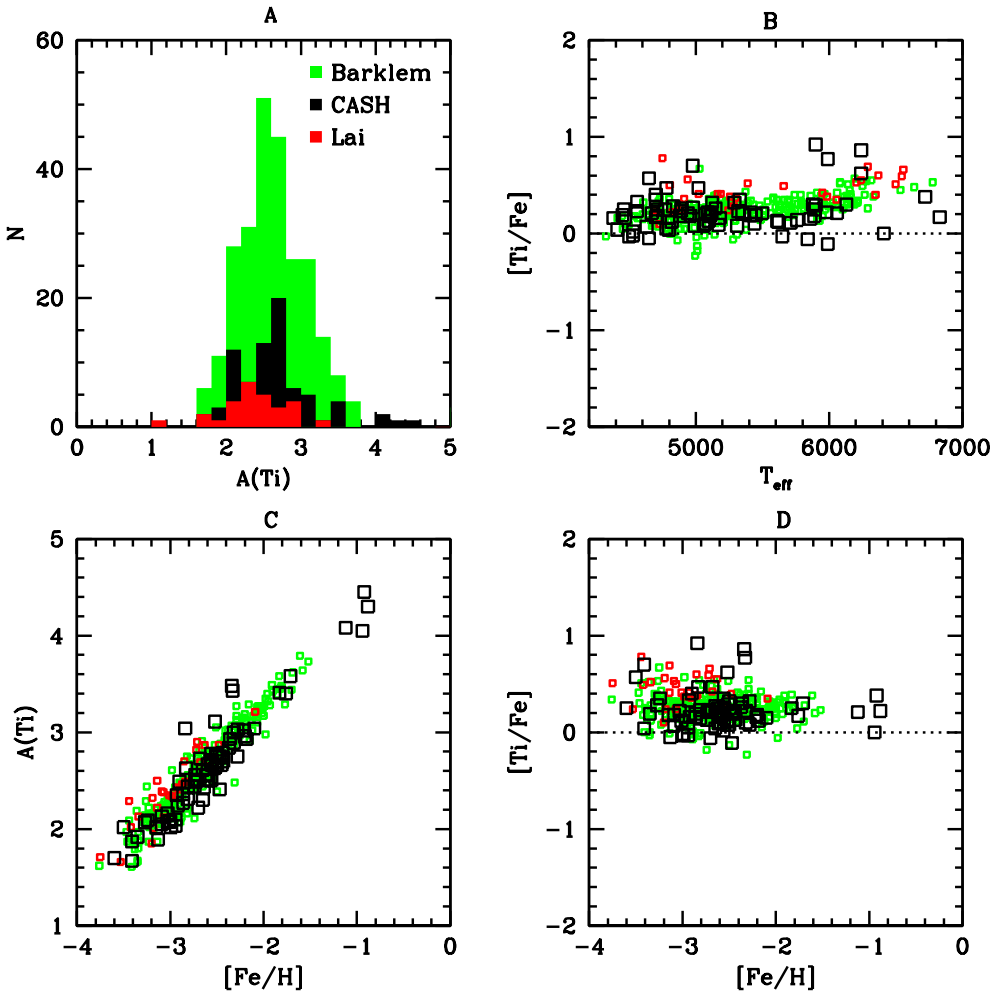

Figure 5.6 Plot of the Ti abundances.

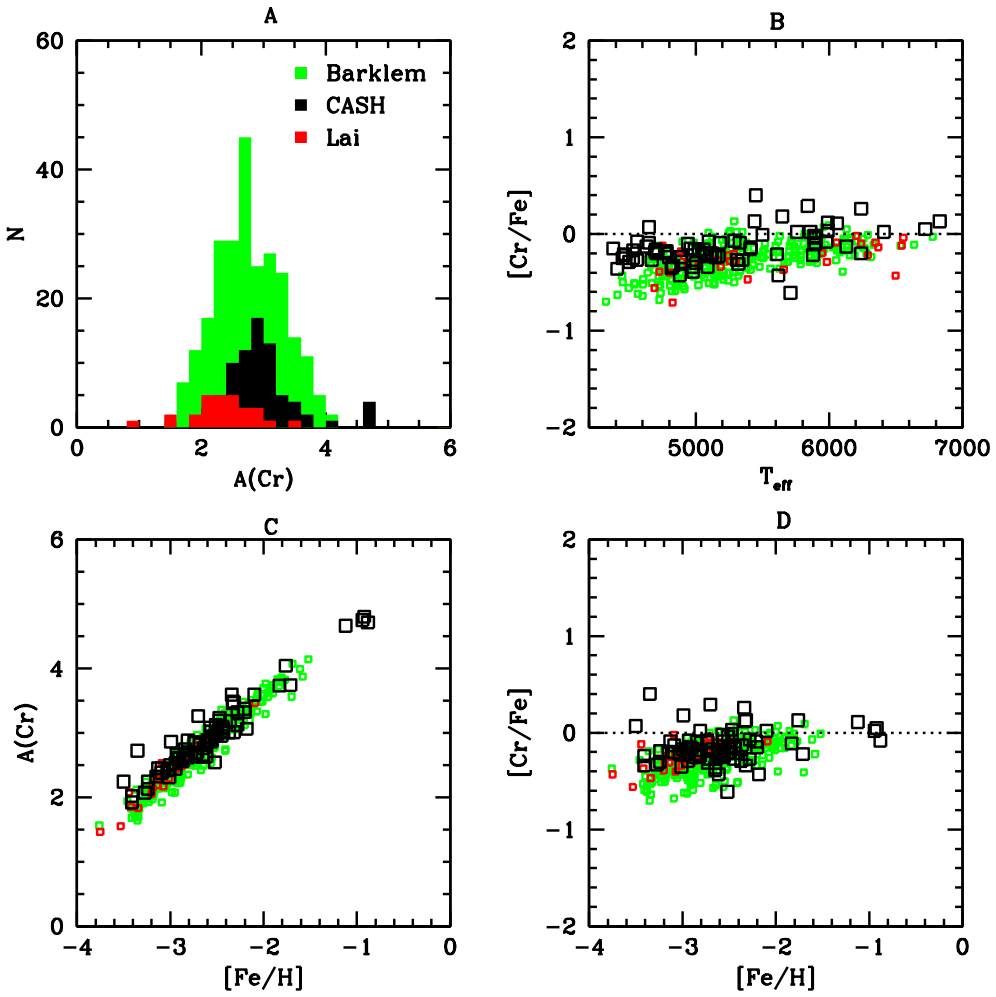

Figure 5.7 Plot of the Cr abundances, which show a trend of decreasing [Cr/Fe] as [Fe/H] decreases.

5476.9 Å and λ 6176.81 Å and often only λ 5476.9 Å is measured, given the S/N constraints. This feature may give spuriously high abundances for Ni.

5.1.4 Neutron Capture Elements: Sr, Ba

The study of the neutron capture elements allows for a test of different sites of nucleosynthesis, beyond proton and α capture in the stellar core. Neutron-capture occurs mainly in two locations in the early universe: in the envelopes of highly evolved asymptotic giant branch stars (s-process) and in some sort of explosive event, likely a core collapse supernova (r-process). Given the resolution and S/N of the CASH data, it is difficult to separate out the r- and s-process contributions. Figures 5.10 and 5.11 show the abundance plots for Sr and Ba.

Strontium provides a probe of the light s-process; however, this is not to say that the r-process does not produce any Sr, but rather its contribution is not nearly as large as the s-process. Abundances are measured via spectral synthesis of the 4215Å line. Traditionally the 4077Å is measured as it is a stronger feature, but it is not within the wavelength regime of the CASH setting. All three studies show a large cosmic scatter in the [Sr/Fe] ratio especially as metallicity decreases with σ_{sd} = 0.62 for CASH, 0.46 for HERES, and 0.56 for Lai.

Barium is thought to be mostly produced in the s-process, with a 20% contribution from the r-process. It may be possible to get a feel for which neutron capture-enhanced stars in CASH are strongly s-process enhanced by evaluating [Ba/Sr], with a large ratio indicating s-process enhancement (Sneden, Cowan, & Galino ARA&A 2008). The Ba abundances are again determined through synthesis of three lines: 4554.04 Å, 5853.69 Å. and 6141.73 Å; however often only the 4554 Å line can be measured given the constraints of the CASH data. The scatter for Ba is also large with σ_{sd} = 0.48 for CASH, 0.70 for HERES, and 0.56 for Lai.

In order to quantify the differences in methodology between HERES and

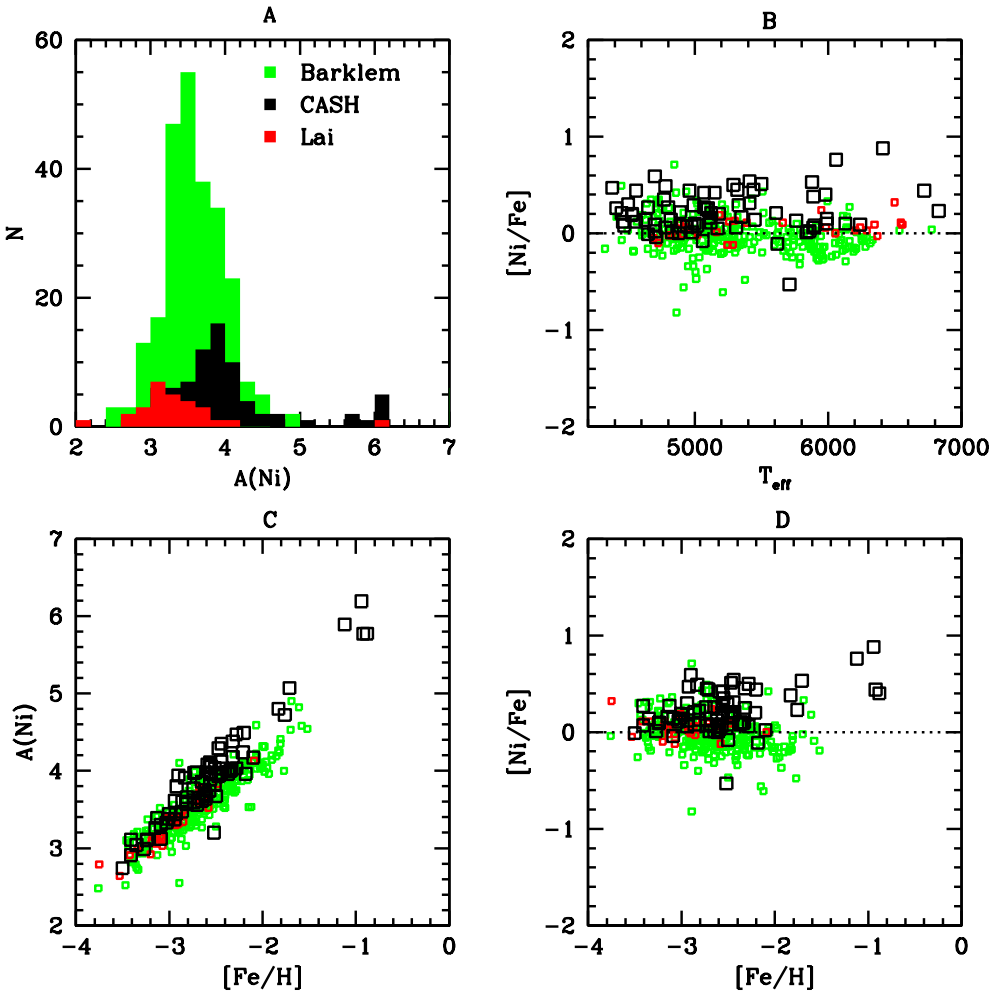

Figure 5.8 Plot of the Ni abundances, which are depleted compared to solar. It should also be noted that there is a discrepancy between the HERES and CASH results. This is likely due to the indicator used to determine Ni abundances in the CASH data.

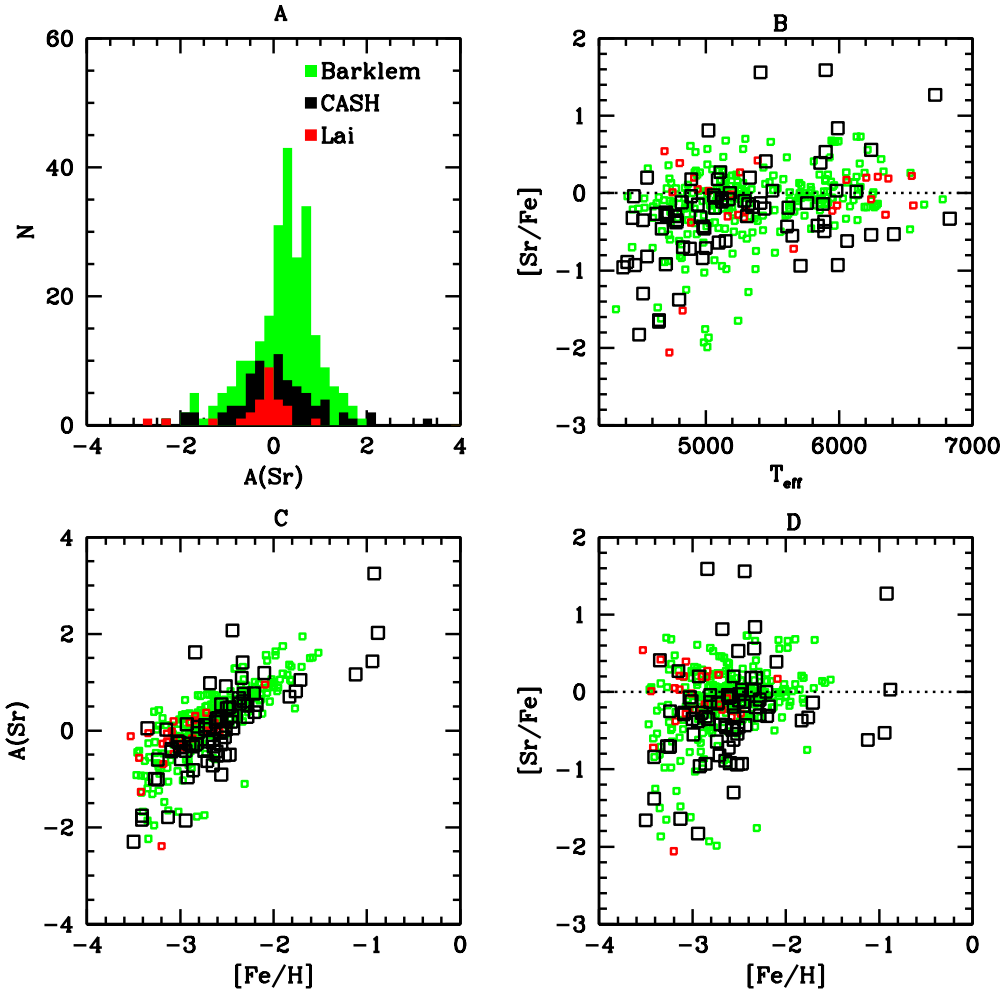

Figure 5.9 Plot of the Sr abundances. Sr shows great spread over 5 orders of magnitude.

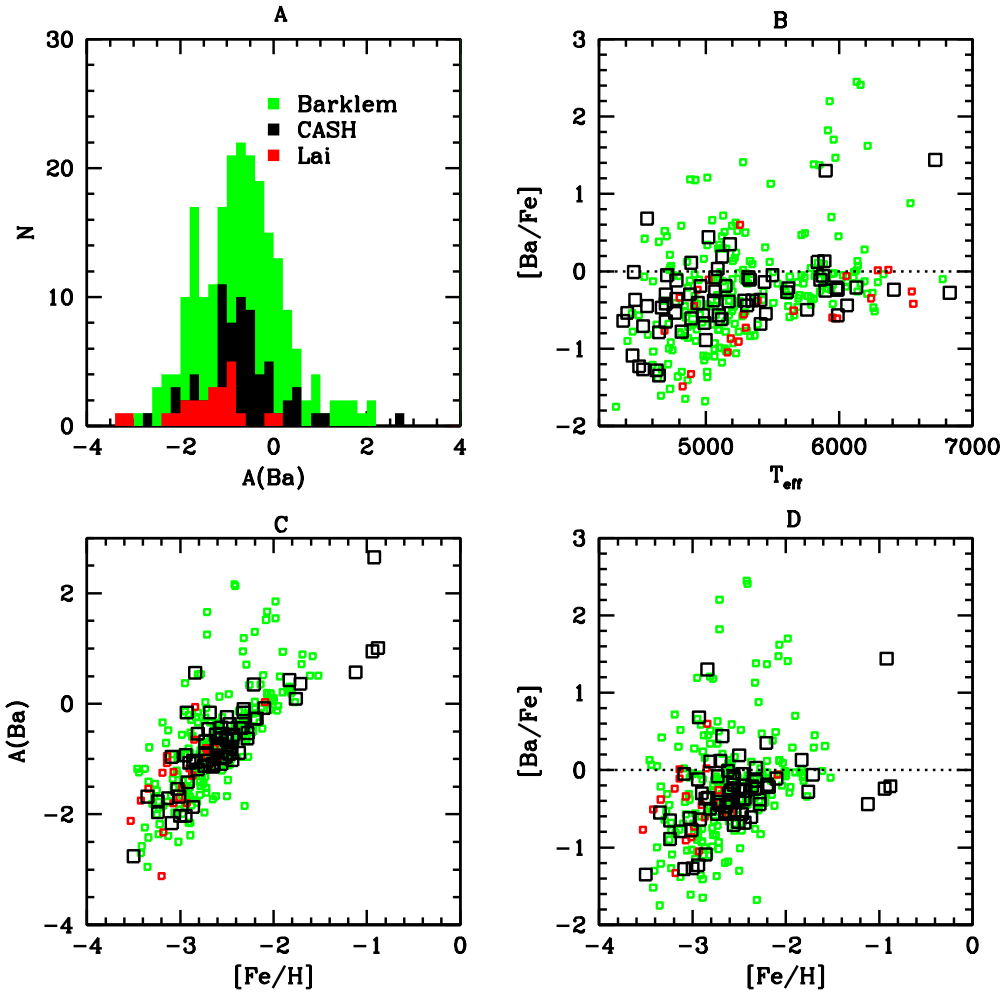

Figure 5.10 Plot of the Ba abundances, which also show great spread over four orders of magnitude.

CASH, a set of HERES spectra will be run though the CASH pipeline to compare the stellar parameters and abundances. In addition, HERES and CASH have one star in common and its stellar parameters and abundances will also aid in the comparison.

Chapter 6

Analysis of Two Newly Discovered EMP stars

The CASH project provides a database of abundances derived from snapshot spectra and from this it is possible to discover interesting stars. Due to the limitations of the CASH project with respect to resolution and S/N, stars that are truly chemically peculiar merit more observations for higher resolution, higher S/N data. Even within the pilot sample, a few chemically peculiar stars have been discovered in the course of evaluating abundances, including a Li-enhanced giant (Roederer et al., 2008).

HE0013-0257 and HE1116-0634 were both observed as part of the CASH program and found to be EMP stars with [Fe/H] = -3.6 and -3.5 respectively. These stars are newly discovered. In fact, aside from the standard stars, the stars selected for CASH currently have no published high resolution abundances. Given the low metallicities of both of these stars, additional data are desired to carefully determine the most complete set of abundances. In addition, this provides an external test of the CASHCODE pipeline and analysis.

6.1 HE0013-0257

HE0013-0257 was observed with the Magellan MIKE instrument at R∼32,000, though this spectrum had never been analyzed prior to its observation in CASH. This star was singled out because its abundances were interesting: it seemed to be slightly C-enhanced, but has deficiencies in the neutron capture elements, with [Sr/Fe]=-0.47 and [Ba/Fe]=-1.23. Combined with its CASH derived metallicity [Fe/H]=-3.6, this star seemed to be similar to the CEMP-no star HE1300+0157 discovered by Frebel et al. (2007, hereby Frebel07) and to the other star discovered in CASH, HE1116-0634.

6.1.1 Stellar Parameters

High resolution MIKE data were then analyzed using the same techniques discussed in Chapter 3. The MIKE data were also run through the CASHCODE pipeline to determine stellar parameters and abundances. Given the overlap in wavelength regimes of MIKE and CASH, there was an opportunity to test the CASHCODE pipeline using many lines that were not measured in the CASH data as well as many lines that were also measured in CASH. A comparison between the stellar parameters derived from the by hand analysis and the pipeline showed good agreement (See Table 6.1). This indicates that the CASHCODE pipeline will yield the same results as a by hand analysis using the same line measurements. A comparison between the CASHCODE pipeline and the MIKE data run through CASHCODE showed similar agreement in the stellar parameters. This shows that the measurements made in the CASH data are reliable. A comparison between the CASH and by hand analysis can be interpreted as a test of both the measurements made from the CASH data and the pipeline against the standard method employed to derive abundances, namely a by hand analysis of high resolution, high S/N data.

Given the differences in spectral coverage of MIKE, blue lines were available

Table 6.1. Comparison of the derived stellar parameters between CASH, MIKE, MIKE+CASHCODE, the blue lines of MIKE, and the blue lines of MIKE+CASHCODE for HE0013-0257

Data	Method	T_{eff}	log g	v_t	[Fe/H]
CASH	CASHCODE	4710	1.35	2.25	-3.60
MIKE	By Hand	4590	0.90	2.05	-3.72
MIKE	CASHCODE	4640	1.00	2.40	-3.62
blue MIKE	By Hand	4650	0.90	2.05	-3.72
blue MIKE	CASHCODE	4540	0.90	2.40	-3.61

for measurement which weren't in CASH data. This allowed us to investigate what effect which lines had been measured had on the stellar parameter derivation. Again, CASH shows good agreement when only the blue lines are used to determine stellar parameters and by the CASHCODE.

The good agreement in the stellar parameters independent of data or method of analysis shows that the low metallicity determined for HE0013-0257 is a robust result.

6.1.2 Abundances

Once it was established that the CASH results were in agreement with the by hand MIKE results (i.e. that measurements made from CASH data and the CASHCODE pipeline gave reliable results), we investigated the differences in the derived abundances. Given the errors on a single star in CASH, agreement within 0.2 dex is considered to be in good agreement. We determined abundances for 6 elements from the equivalent width: Mg, Ca, Ti, Cr, Fe, and Ni and 4 by synthesis: Li, C, Sr, and Ba. Table 6.2 lists the abundances determined in the CASHCODE pipeline for the CASH data and Table 6.3 lists the abundances determined by hand for the MIKE data. In the case of Li in table 6.2 [Li/Fe] is not what is listed, but rather the offset of the Li abundance with respect to the Spite plateau is quoted. Figure

Table 6.2. CASH derived abundances for HE0013-0257

Element	logϵ(X)	[X/Fe]	Err
Li I	0.12	-2.08*	0.25
CH	5.35	0.39	0.30
Mg I	4.53	0.55	0.10
Ca I	3.10	0.34	0.10
Ti I	1.66	0.27	0.10
Ti II	1.70	0.25	0.12
Cr I	1.83	-0.24	0.15
Ni I	2.86	0.21	0.25
Sr II	-1.11	-0.41	0.25
Ba II	-2.64	-1.17	0.31

Table 6.3. MIKE derived abundances for HE0013-0257

Element	logϵ(X)	[X/Fe]	Err
CH	5.01	0.17	0.15
Mg I	4.43	0.57	0.11
Ca I	3.00	0.36	0.09
Ti I	1.56	0.29	0.17
Ti II	1.60	0.33	0.12
Cr I	1.58	-0.37	0.23
Ni I	2.67	0.14	0.13
Sr II	-1.10	-0.28	0.10
Ba II	-2.57	-0.98	0.10

6.1 is a representation of Tables 6.1 and 6.2, showing the differences in abundances derived by hand for the MIKE data, the abundances derived with the CASHCODE pipeline from MIKE data, and the abundances derived from CASH data with the CASHCODE pipeline.

α Elements

Mg and Ca seem to match well between the by hand and MIKE pipeline results. This is to be expected because the same measurements of the same lines were used. Deviations seen in Mg between CASH and the by hand analysis likely arise from the inclusion of blue lines of Mg which can yield lower abundances than the strong

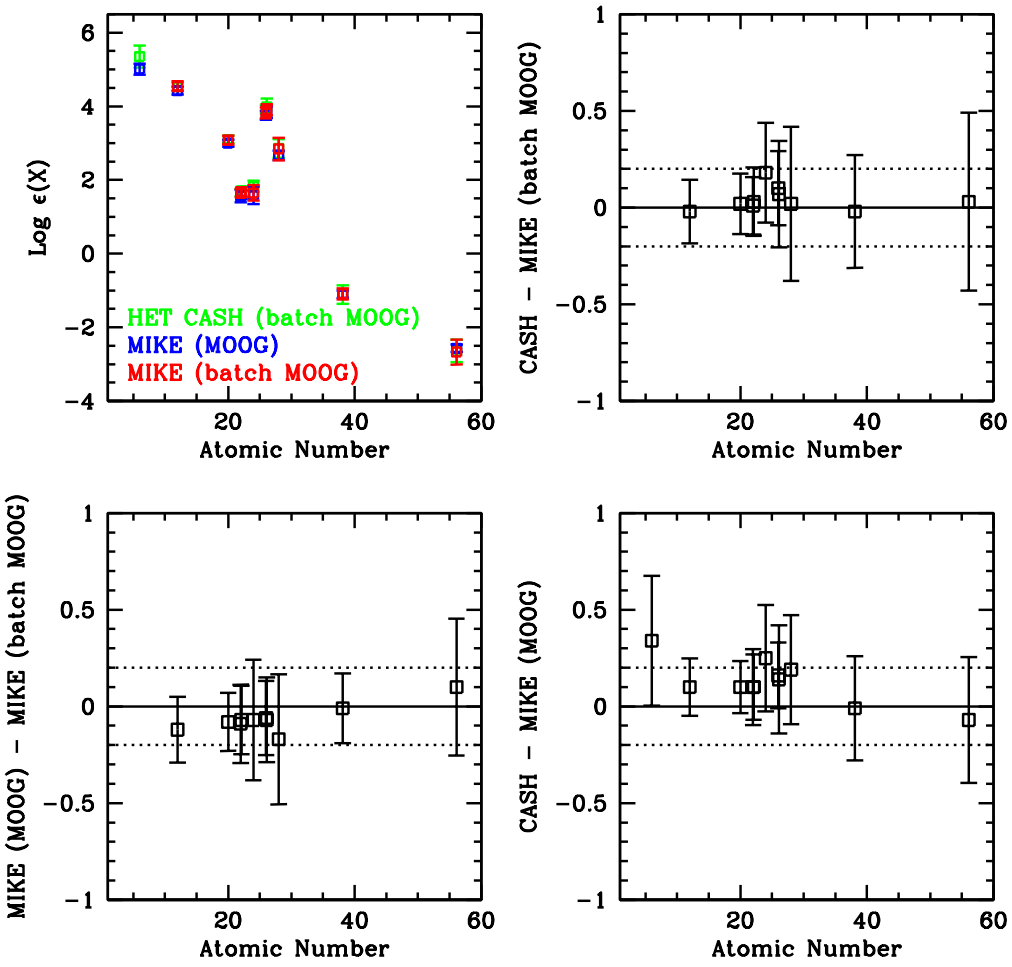

Figure 6.1 Plot of the abundances derived between CASH and high resolution data. In the upper left panel is plotted the log ϵ abundances derived against the atomic number. Green points are the ones derived from CASH, red points are derived from MIKE data using the CASHCODE pipeline, and the blue points are the abundances determined from a by hand analysis. In the upper right panel are the residuals of the different log ϵ abundances derived from CASH and the MIKE data using the CASHCODE pipeline plotted against atomic number. The remaining two panels are similar. In the bottom left panel is the comparison between the by hand analysis of the MIKE data with the CASHCODE pipeline analysis of MIKE data and in the bottom right panel is the comparison between CASH and the by hand analysis for the MIKE data.

lines measured in CASH, which can fall on the non-linear portion of the curve of growth. In general, Mg and Ca are overabundant compared to solar, which is what is has been observed for metal-poor stars (e.g. Cayrel et al. (2004)).

Ti, which is being considered with the α elements, matches well between Ti I and Ti II and also between the different data and methods of analysis showing a slight enhancement with [Ti/Fe]= 0.26 from CASH data and 0.31 from MIKE data. The ratio appears to be consistent for what is expected at low metallicity (e.g. McWilliam (1997)).

Fe Peak Elements

Fe abundances are calculated as part of the stellar parameter determination and match well between the by hand, MIKE pipeline, and CASH analysis.

Chromium shows a large deviation. There are some Cr features that give spurious results due to blending; however, once these lines were taken out of the line list the abundances all seemed to match better. The difficulty in determining Cr abundances are the number of available lines in the wavelength region given the resolution and S/N of the CASH data. There are many more available lines in the MIKE data, creating some offset between the abundances. Both the by hand analysis and CASH analysis show [Cr/Fe] to be sub-solar, which is what has been found at the lowest metallicities (e.g. McWilliam (1997))

Nickel presented problems and as discussed earlier, there are only two Ni features in CASH with the prominent feature λ 5476Å often being the only available line. This line may give comparatively high abundances, so the Ni abundance for this star and the rest of CASH is presented with a large error.

Neutron Capture Elements

The abundances of Sr and Ba were based upon spectral synthesis. For Sr, the 4215 Å line was used, as it is a strong feature. Measurement of the 4077Å line in the MIKE data is currently in progress. There is good agreement between the by hand and automated syntheses.

The 4554 Å line of Ba II was used to determine the Ba abundance. There is also good agreement in the Ba abundances. This is, again, a strong feature. Given the low neutron capture abundances in this star, only the strongest features will be present. A consideration must also be made for the very low metallicity of the star as well: generally, as metallicity decreases so do the absolute abundances of the other elements. The neutron capture elements show greater scatter at any given metallicity compared to, for example the α elements, but there is still a decrease in the logϵ abundances of the neutron capture elements as metallicity decreases. Thus, for low metallicity and low neutron capture abundances, only the strongest features can be measured.

Carbon

Since the C synthesis is done by hand, there is no comparison between the CASH-CODE pipeline and the by hand synthesis. Evaluation of the differences between the two by hand syntheses reflect the quality of the abundances which can be derived at low resolution and low S/N as compared to high resolution and high S/N. C shows the largest deviation of all the elements, but the fit of the spectral synthesis to the high resolution data is much better. Thus, errors quoted along side the CASH abundances are high due to the S/N of the C region.

6.2 HE1116-0634

HE1116-0634 was observed with the AAT UCLES instrument at R∼16000; however, the data were never analyzed prior to the CASH study. This star was subsequently observed as part of CASH and singled out for its low metallicity. Similar to HE0013-0257 and the CEMP-no star HE1300+0157, this star shows a slight carbon enhancement with [C/Fe] = 0.35 and neutron capture depletion, with [Sr/Fe] = -1.66 and [Ba/Fe] = -1.35 thus providing for a good basis of comparison.

6.2.1 Stellar Parameters

Stellar parameters and abundances were determined for this star three ways: with CASH data through the CASHCODE pipeline, with AAT data through the CASHCODE pipeline, and with AAT data by hand.

A similar analysis to the one performed on HE0013-0257 was conducted for the stellar parameters for HE1116-0634. See Table 6.4. There is good agreement between the effective temperatures, gravities, and metallicities. There is a discrepancy in the CASH value and the AAT values in microturbulence, but this may be attributed to the fact that there are fewer lines being measured to determine the parameters in CASH than in the AAT data. As stated in Chapter 2, the wavelength regime for the UCLES instrument is far bluer than that of CASH. From the MIKE analysis, it appears that the abundances derived with only the blue lines give results within the standard errors, but the differences in lines chosen will likely affect other elements with fewer features more than Fe and Ti. However, it should be stated that this large discrepancy in microturbulence will have an effect on the final abundances. We are currently investigating the cause of this difference.

It is also seen in both HE0013-0257 and HE1116-0634 that CASH derived surface gravities are higher than those in the higher resolution data. This may be due to the fact that in the CASH data there are only three reliable Fe II lines which

Table 6.4. Comparison of the derived stellar parameters between CASH, AAT, and AAT+CASHCODE

Data	Method	T_{eff}	log g	v_t	[Fe/H]
CASH	CASHCODE	4650	1.00	3.80	-3.50
AAT	By Hand	4650	0.80	2.00	-3.53
AAT	CASHCODE	4600	0.80	2.00	-3.41

Table 6.5. CASH derived abundances for HE1116-0634

Element	logϵ(X)	[X/Fe]	Err
CH	5.39	0.35	0.30
Mg I	4.22	0.14	0.46
Ca I	3.07	0.21	0.10
Ti I	1.76	0.27	0.21
Ti II	2.02	0.57	0.19
Cr I	2.11	-0.06	0.21
Ni I	2.74	-0.01	0.25
Sr II	-2.30	-1.66	0.25
Ba II	-2.76	-1.35	0.25

are sufficiently unblended at R$\sim$15000.

6.2.2 Abundances

This again provided an opportunity to compare CASH abundances derived with those abundances derived with higher resolution data. Again, the difference in microturbulence combined with the different sets of available lines due to wavelength are also things that could cause discrepancies in the derived abundances, thus the following set of abundances are preliminary.

Tables 6.5 and 6.6 show the abundances derived with the CASH data and derived by hand from the AAT data. These are both represented along with abundances derived with the AAT data using the CASHCODE pipeline in Figure 6.2.

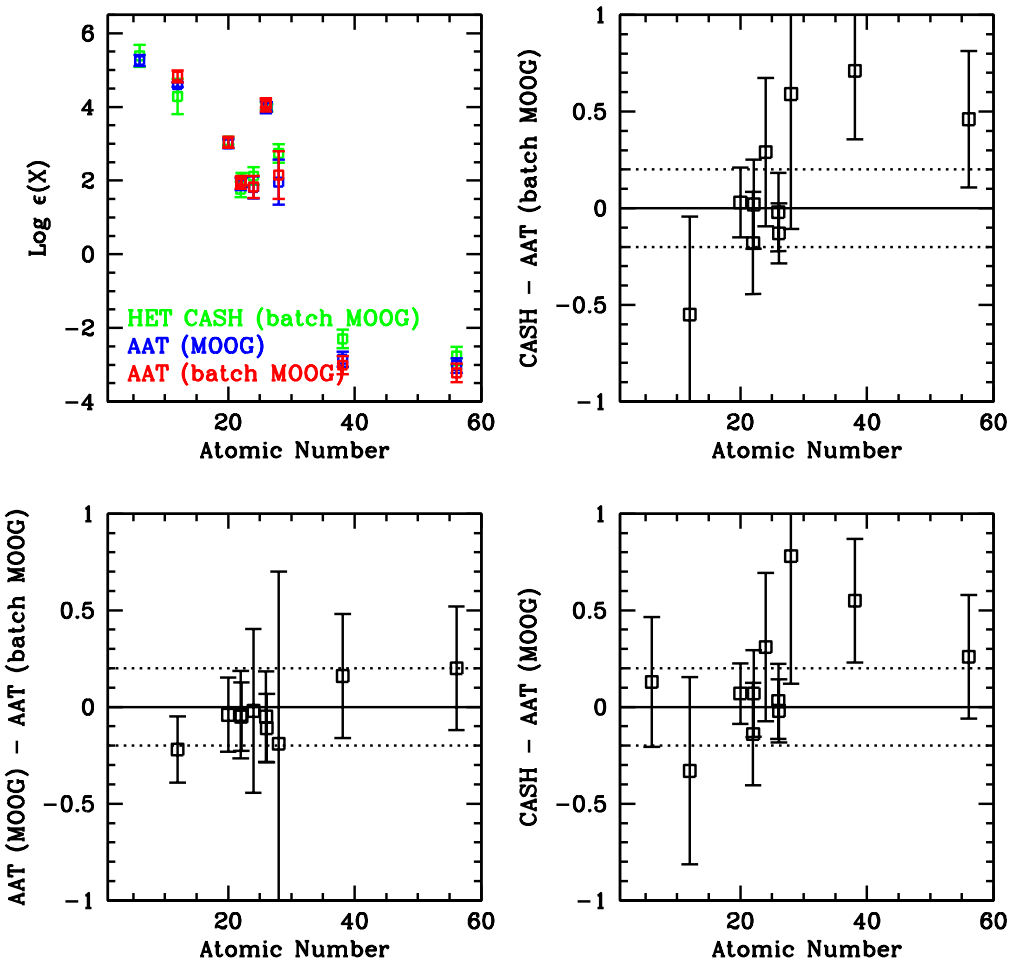

Figure 6.2 Comparison of CASH log ϵ abundances for HE1116-0634 with AAT logϵ abundances. The panels are the same as in Figure 6.1. In the upper left hand corner is plotted the logϵ abundances versus atomic number. In green are the CASH derived abundances, in red are the AAT CASHCODE pipeline analysis abundances, and in blue is the by hand analysis of the AAT data.

Table 6.6. AAT derived abundances for HE1116-0634

Element	logϵ(X)	[X/Fe]	Err
CH	5.26	0.23	0.15
Mg I	4.61	0.56	0.06
Ca I	3.00	0.17	0.12
Ti I	1.90	0.44	0.16
Ti II	1.95	0.49	0.12
Cr I	1.81	-0.33	0.30
Ni I	1.96	-0.76	0.61
Sr II	-2.85	-2.22	0.20
Ba II	-3.02	-1.62	0.20

α Elements: Mg, Ca, Ti

The α elements are all shown to be enhanced relative to solar. There is disagreement between the derived values of [Mg/Fe] between the CASH data and the AAT data, with [Mg/Fe] = 0.14 and 0.56 from CASH and the AAT respectively. This discrepancy could be the result of which Mg lines were used, but a better determination of the [Mg/Fe] ratio requires higher S/N data than that of the CASH or AAT. Given that this star is an EMP, its lines are weak hence higher S/N is required to do a comparable analysis of a star with higher metallicity. Ca is in good agreement between the two data sets, with [Ca/Fe] = 0.21 and 0.17 from the CASH data and the AAT data. Ti is in agreement between the CASH data derived abundance and the AAT data derived abundance; however, there is disagreement between Ti I and Ti I in the CASH data. This is likely due to the lack of Ti I lines. The AAT data spans the blue portion of the spectrum where more Ti I lines can be found. In addition, as in the case of the Mg lines, the low metallicity of this star also makes it difficult to measure these weakened features.

Fe Peak Elements: Cr, Ni

Cr is shown to be slightly underabundant compared to solar in CASH with [Cr/Fe]=-0.06. The AAT data derived abundance ratio is lower with [Cr/Fe]=-0.33. This sort of depletion is expected at these metallicities (McWilliam, 1997).

The Ni abundance in CASH is substantially higher, with [Ni/Fe]= -0.01, than that of the AAT data, at [Ni/Fe]=-0.76. Only one Ni line was available for the CASH analysis, which seems to give high Ni abundances. The three Ni lines in the AAT data vary widely, giving a large uncertainty on the derived abundance; however these reasons do not explain the entire 0.75 dex discrepancy, so tests are in progress to understand the difference in abundances. Also, compared to the rest of the CASH sample, the Ni abundance is, indeed, low.

Neutron Capture Elements: Sr, Ba

The greatest discrepancy is seen at the neutron capture elements. Both Ba and Sr are synthesized using the 4554Å and 4215Å lines respectively. The cause for the discrepancy is not due to the pipeline, but rather the data. The AAT abundances for the by hand and CASHCODE analyses give similar abundances, but both differ greatly with CASH. This is due to problems in the order merging for the AAT data. Both the 4554 Å Ba line and the 4215Å Sr lines fall near the end of the order, which trail off and then jump up at the beginning of the next order. These data will be reanalyzed in their individual orders to remove this artifact, in addition to the inclusion of the 4077Å Sr line.

Carbon

The C abundances derived between the CASH data and the AAT data agree well, within 0.13 dex. Both indicate that HE1116-0634 is slightly carbon enhanced compared to solar with the CASH data derived abundance ratio being [C/Fe] = 0.39

and the AAT data derived abundance ratio being 0.23, though it is not technically a CEMP because [C/Fe] < 1.

6.3 Interpretation

HE0013-0257 and HE1116-0634 are remarkably similar in their abundance patterns. Both show a slight C enhancement, α-enhancement, Fe peak depletion, and extreme neutron capture depletion. The abundance patterns for both stars somewhat resemble the abundance patterns in CEMP-no stars. In particular, their abundance patterns are similar to that of HE1300+0157 (Frebel et al., 2007). To provide context, Figure 6.3 shows the abundances of selected elements in HE1300+0157 plotted with the CASH data abundances (black open squares), and the CASH data derived abundances of HE0013-0257 (green squares), and HE1116-0634 (red squares).

Neither of these stars can be considered a CEMP since [C/Fe] for both is less than 1.0; however, they are both C enhanced relative to solar. The production mechanism for this addition C must be independent from the production mechanism for the neutron capture elements. Specifically, no s-process enhancement is seen and it is unlikely that r-process has contributed as well. It is unknown what this mechanism is. Given that these stars both have [Fe/H] <-3.5, they belong to an small set of stars (perhaps no more than 20), which have been discovered to date. They provide an indirect probe of the early universe, likely having formed with very few previous generations of star formation and death.

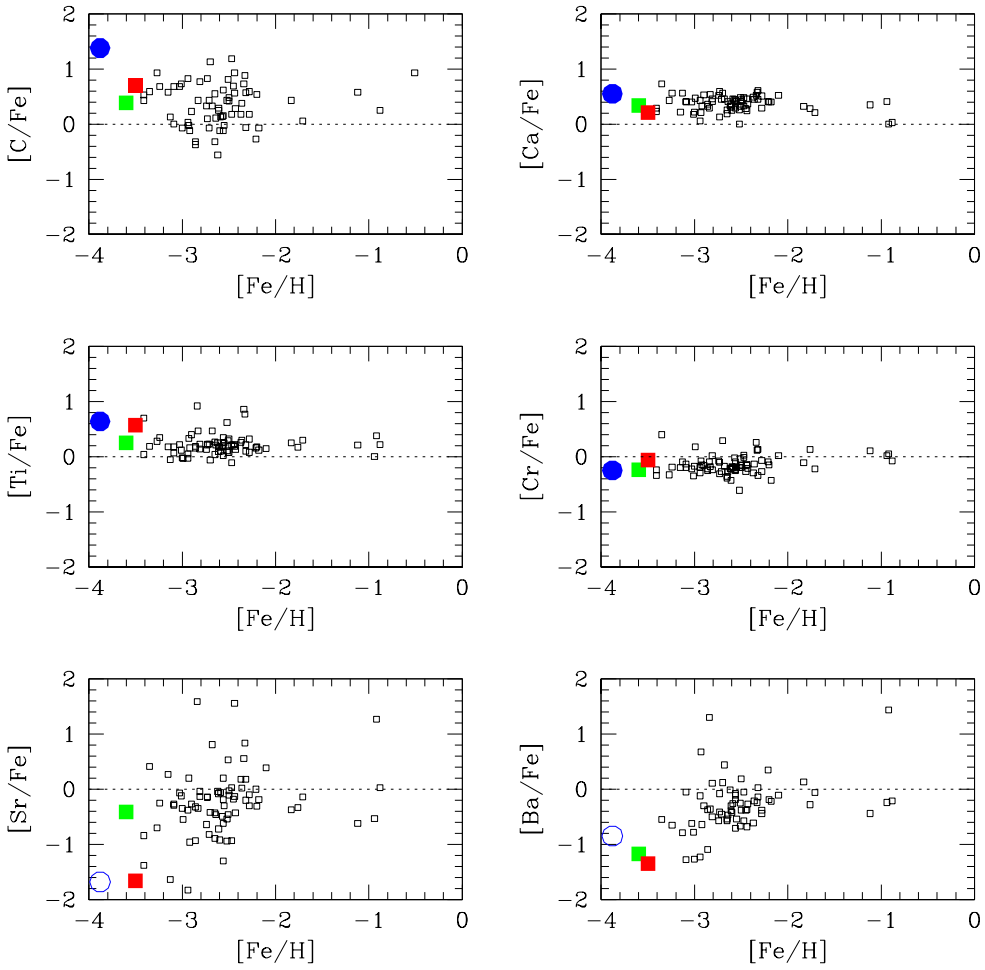

Figure 6.3 In this figure the CASH determined abundances for the entire sample are plotted as small black open boxes in the background of three symbols: the green filled square corresponds to the CASH abundances of HE0013-0257, the red filled square corresponds to the CASH abundances of HE1116-0634, and the blue filled circle corresponds to the subgiant abundances for HE1300+0157 from Frebel07 and the blue open circle corresponds to upper limits determined from Frebel07

Chapter 7

Conclusions

The CASH project is a large scale study aimed at characterizing the chemical abundance trends and frequencies of the stellar halo. When completed, it will be the largest set of high resolution abundances for metal-poor stars and will bring the study of metal-poor stars well beyond the low number statistics regime. In this paper we present results on the first 80 stars, designated as a pilot sample to help develop and calibrate a stellar parameter and abundance pipeline. The size of this sample is also significant, as it is the second largest set of high resolution abundances to date. Abundance trends for eleven elements are presented.

The CASH project will not only provide a database from which trends and frequencies will be determined, but will also serve as a means of discovering new and astrophysically interesting metal-poor stars. Two such stars have already been discovered in the CASH sample: HE0013-0257 and HE1116-0634. These stars both have metallicities below -3.5 dex, adding to the $\sim$20 known [Fe/H]$<$-3.5 stars.

Future Work

The data processing for the CASH project will be finished over the course of the summer, expanding the number of stars to $\sim$500. With the completed set of abun-

dances, trends will be reexamined and frequencies of chemically deviant groups of stars can be assessed. The set of CASH abundances will be compared to supernova yields to indirectly probe progenitor masses of supernova in the early universe.

It is also expected that more chemically peculiar individual stars will be discovered, for which additional observations at higher resolution and higher S/N will be taken such that the most complete set of abundances can be determined for these objects.

Follow up observations, which have already begun, revealed that HE0434+0105 is a double lined spectroscopic binary star. Spectral analysis to derive a set of abundances from each component will be performed to see whether or not their abundances match.

Bibliography

Adelman-McCarthy, e. a. 2008, ApJS, 175, 297

Adelman-McCarthy, J. K., e. a. 2006, ApJS, 162, 38

Aoki, W., Beers, T. C., Christlieb, N., Norris, J. E., Ryan, S. G., & Tsangarides, S. 2007, ApJ, 655, 492

Barklem, P. S., Christlieb, N., Beers, T. C., Hill, V., Bessell, M. S., Holmberg, J., Marsteller, B., Rossi, S., Zickgraf, F.-J., & Reimers, D. 2005, A&A, 439, 129

Beers, T. C. & Christlieb, N. 2005, ARA&A, 43, 531

Beers, T. C., Preston, G. W., & Shectman, S. A. 1985, AJ, 90, 2089

—. 1992, AJ, 103, 1987

Beers, T. C., Rossi, S., Norris, J. E., Ryan, S. G., & Shefler, T. 1999, AJ, 117, 981

Bernstein, R., Shectman, S. A., Gunnels, S. M., Mochnacki, S., & Athey, A. E. 2003, in Society of Photo-Optical Instrumentation Engineers (SPIE) Conference Series, ed. M. Iye & A. F. M. Moorwood, Vol. 4841, 1694–1704

Bromm, V., Coppi, P. S., & Larson, R. B. 1999, ApJ, 527, L5

Cassisi, S., Castellani, M., Caputo, F., & Castellani, V. 2004, A&A, 426, 641

Castelli, F. & Kurucz, R. L. 2004, ArXiv Astrophysics e-prints

Cayrel, R., Depagne, E., Spite, M., Hill, V., Spite, F., François, P., Plez, B., Beers, T., Primas, F., Andersen, J., Barbuy, B., Bonifacio, P., Molaro, P., & Nordström, B. 2004, A&A, 416, 1117

Christlieb, N. 2003, Rev. Mod. Astron., 16, 191

Christlieb, N., Wisotzki, L., Reimers, D., Homeier, D., Koester, D., & Heber, U. 2001, A&A, 366, 898

Frebel, A., Aoki, W., Christlieb, N., Ando, H., Asplund, M., Barklem, P. S., Beers, T. C., Eriksson, K., Fechner, C., Fujimoto, M. Y., Honda, S., Kajino, T., Minezaki, T., Nomoto, K., Norris, J. E., Ryan, S. G., Takada-Hidai, M., Tsangarides, S., & Yoshii, Y. 2005, Nature, 434, 871

Frebel, A., Christlieb, N., Norris, J. E., Beers, T. C., Bessell, M. S., Rhee, J., Fechner, C., Marsteller, B., Rossi, S., Thom, C., Wisotzki, L., & Reimers, D. 2006, ApJ, 652, 1585

Frebel, A., Norris, J. E., Aoki, W., Honda, S., Bessell, M. S., Takada-Hidai, M., Beers, T. C., & Christlieb, N. 2007, ApJ, 658, 534

Fulbright, J. P. 2000, AJ, 120, 1841

García Pérez, A. E., Asplund, M., Primas, F., Nissen, P. E., & Gustafsson, B. 2006, A&A, 451, 621

Ivans, I. I., Sneden, C., James, C. R., Preston, G. W., Fulbright, J. P., Höflich, P. A., Carney, B. W., & Wheeler, J. C. 2003, ApJ, 592, 906

Kim, Y.-C., Demarque, P., Yi, S. K., & Alexander, D. R. 2002, ApJS, 143, 499

Lai, D. K., Bolte, M., Johnson, J. A., Lucatello, S., Heger, A., & Woosley, S. E. 2008, ApJ, 681, 1524

Lee, Y. S., Beers, T. C., Sivarani, T., Allende Prieto, C., Koesterke, L., Wilhelm, R., Norris, J. E., Bailer-Jones, C. A. L., Re Fiorentin, P., Rockosi, C. M., Yanny, B., Newberg, H., & Covey, K. R. 2007, ArXiv e-prints, 710

Masseron, T., Johnson, J. A., Plez, B., van Eck, S., Primas, F., Goriely, S., & Jorissen, A. 2010, A&A, 509, A93+

McWilliam, A. 1997, ARAA, 35, 503

Meléndez, J. & Barbuy, B. 2009, A&A, 497, 611

Nilsson, H., Ljung, G., Lundberg, H., & Nielsen, K. E. 2006, A&A, 445, 1165

Norris, J. E., Ryan, S. G., & Beers, T. C. 1996, ApJS, 107, 391

Norris, J. E., Ryan, S. G., Beers, T. C., Aoki, W., & Ando, H. 2002, ApJ, 569, L107

Piskunov, N. E. & Valenti, J. A. 2002, A&A, 385, 1095

Roederer, I. U., Frebel, A., Shetrone, M. D., Allende Prieto, C., Rhee, J., Gallino, R., Bisterzo, S., Sneden, C., Beers, T. C., & Cowan, J. J. 2008, ApJ, 679, 1549

Roederer, I. U., Sneden, C., Thompson, I. B., Preston, G. W., & Shectman, S. A. 2010, ApJ, 711, 573

Ryan, S. G., Beers, T. C., Deliyannis, C. P., & Thorburn, J. A. 1996, ApJ, 458, 543

Sivarani, T., Bonifacio, P., Molaro, P., Cayrel, R., Spite, M., Spite, F., Plez, B., Andersen, J., Barbuy, B., Beers, T. C., Depagne, E., Hill, V., François, P., Nordström, B., & Primas, F. 2004, A&A, 413, 1073

Sneden, C., McWilliam, A., Preston, G. W., Cowan, J. J., Burris, D. L., & Amorsky, B. J. 1996, ApJ, 467, 819

Sneden, C. A. 1973, PhD thesis, The University of Texas at Austin

Sobeck, J. S., Lawler, J. E., & Sneden, C. 2007, ApJ, 667, 1267

Spite, F. & Spite, M. 1982, A&A, 115, 357

Tull, R. G. 1998, in Society of Photo-Optical Instrumentation Engineers (SPIE) Conference, Vol. 3355, Optical Astronomical Instrumentation, ed. S. D'Odorico, 387

van Dokkum, P. G. 2001, PASP, 113, 1420

Vita

Permanent Address: 9611 Magna Carta Loop
Austin, TX 78754

This thesis was typeset with LaTeX 2$_\varepsilon$[1] by the author.

[1] LaTeX 2$_\varepsilon$ is an extension of LaTeX. LaTeX is a collection of macros for TeX. TeX is a trademark of the American Mathematical Society. The macros used in formatting this thesis were written by Dinesh Das, Department of Computer Sciences, The University of Texas at Austin, and extended by Bert Kay, James A. Bednar, and Ayman El-Khashab.